Supplement of Atmos. Chem. Phys., 18, 4765–4801, 2018
https://doi.org/10.5194/acp-18-4765-2018-supplement

Atmospheric Chemistry and Physics
Open Access
EGU

Supplement of

Estimates of CO_2 fluxes over the city of Cape Town, South Africa, through Bayesian inverse modelling

Alecia Nickless et al.

Correspondence to: Alecia Nickless (alecia.nickless@phc.ox.ac.uk)

1 Supplementary Material

1.1 CO_2 Measurements

A single calibration standard was kept at each site, and run periodically in order to assess whether any drift occurred in the CO_2 measurements over time, to determine if the calibration coefficients required any adjustment. At Robben Island the measurements of the calibration standard were (mean $\pm$ (standard deviation)) 386.89 ppm ($\pm$ 0.014) in November, 385.67 ppm ($\pm$ 0.012) in February 2013, and 385.73 ppm ($\pm$ 0.012) in June 2013. This indicates that the instrument was making stable measurements during the sixteen month campaign. The slightly higher reading in November 2012 occurred when the weather was wet, and there was more moisture contamination from the previous ambient measurements prior to calibration. At Hangklip the instrument measured the calibration standard at 378.26 ppm ($\pm$ 0.009) in November 2012 and at 378.16 ppm ($\pm$ 0.022) in June 2013, indicating no evidence of drift over the measurement period.

In addition to each site's calibration standard, a travelling reference standard was also measured at close proximity in time at all three sites, including Cape Point. This standard consisted of clean air collected at the Cape Point site. The results of two of these calibration measurements are presented in Table S1. By comparing calibration measurements with Cape Point inter-site differences are ensured to be negligible, and also links the Robben Island and Hangklip sites into the greater GAW network. The instruments at Cape Point are routinely calibrated with standards shared around the GAW network, which maintains high levels of quality control. Differences were found to be small between sites, and between calibration periods using the same standard in June 2012 and June 2013.

Table S1. Mean and standard deviation of CO_2 measurements (ppm) during calibration phase using a travelling CO_2 standard (June 2012 and June 2013) traceable to several Cape Point CO_2 laboratory standards. These in turn are linked to primary CO_2 standards maintained at the NOAA calibration laboratory in Boulder, USA.

FA01830	Site			
Date	Cape Point	Robben Island	Hangklip	Maximum inter-site difference
June 2012	452.77 (0.03)	452.88 (0.02)	452.89 (0.03)	0.12
June 2013	452.28 (0.03)	452.86 (0.02)	452.60 (0.03)	0.58
June 2012 - June 2013	0.49	0.02	0.29	

The observed hourly CO_2 concentrations at the Robben Island and Hangklip sites are presented in Figure S1, together with the hourly measurements at Cape Point and the measured daily temperature at this site. There is no clear correlation between the peaks in CO_2 and daily temperature. From March 2012 until June 2013, the mean CO_2 concentration observed at Robben Island was 391.3 ppm ($\pm$ 5.02), usually ranging between 389.5 and 394.2 ppm, with a minimum of 382.4 ppm and a maximum of 445.0 ppm. The measurements at Hangklip had a similar mean of 390.6 ppm ($\pm$ 3.89), usually ranging between 389.5 and 391.4 ppm with a minimum of 380.4 ppm and a maximum of 430.6 ppm. The Cape Point measurements have a narrower range of 382.9 to 412.3 ppm, with a mean of 392.1 ppm, indicating less influence from local sources and sinks.

The mean diurnal cycle for each month is presented in Figure S2. Across all months, the diurnal cycle of CO_2 concentrations at Cape Point are relatively flat compared with Robben Island and Hangklip. In November 2012 and February 2013 the diurnal cycle for both measurement sites was the most flat. This is the summer period, when temperatures are high and the Western Cape experiences the lowest amount of rain. The amplitude of the diurnal cycle at both sites increased from April, reaching a maximum amplitude in June and July. This is during the winter rainfall period in the Western Cape. Temperatures are mild and much of the vegetation growth occurs during this period. The diurnal cycle of the Hangklip site dipped below both Cape Point and Robben Island, indicating that this site is more affected by local sinks of CO_2. Robben Island consistently had the highest peaks in CO_2 concentrations across all months, indicating that this site was the most affected by local sources, which is what we expected.

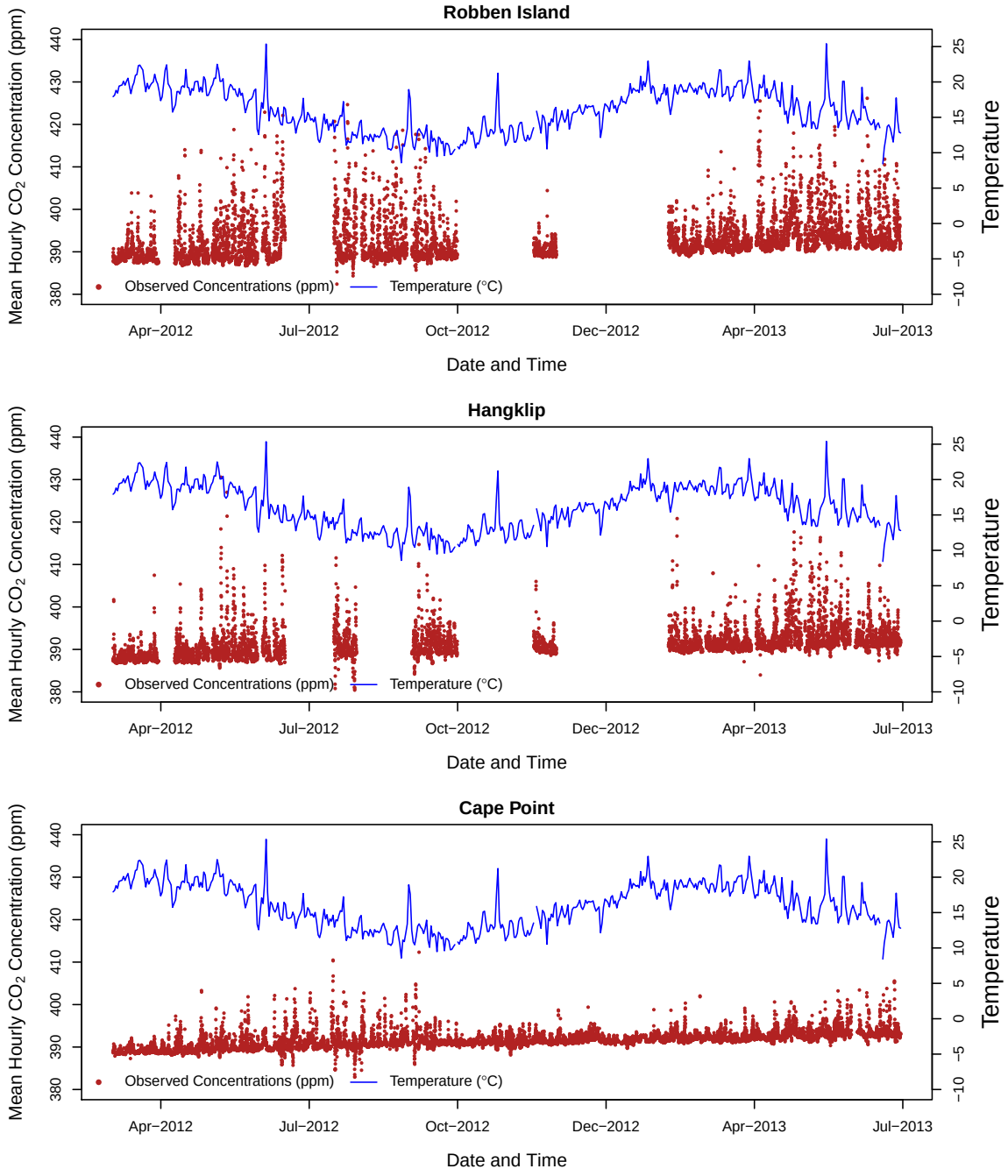

Figure S1. Observed hourly CO_2 concentrations (ppm) (left-side axis) at the Robben Island (top closed red circles) and Hangklip (bottom closed black circles) measurement sites. The blue line appearing at the bottom of each plot is the CO_2 concentration measurements at Cape Point station (ppm) and the green line at the top of each plot is the mean daily temperature $(^{\circ}C)$ as measured at the Cape Point station, which is represented by the right-side axis.

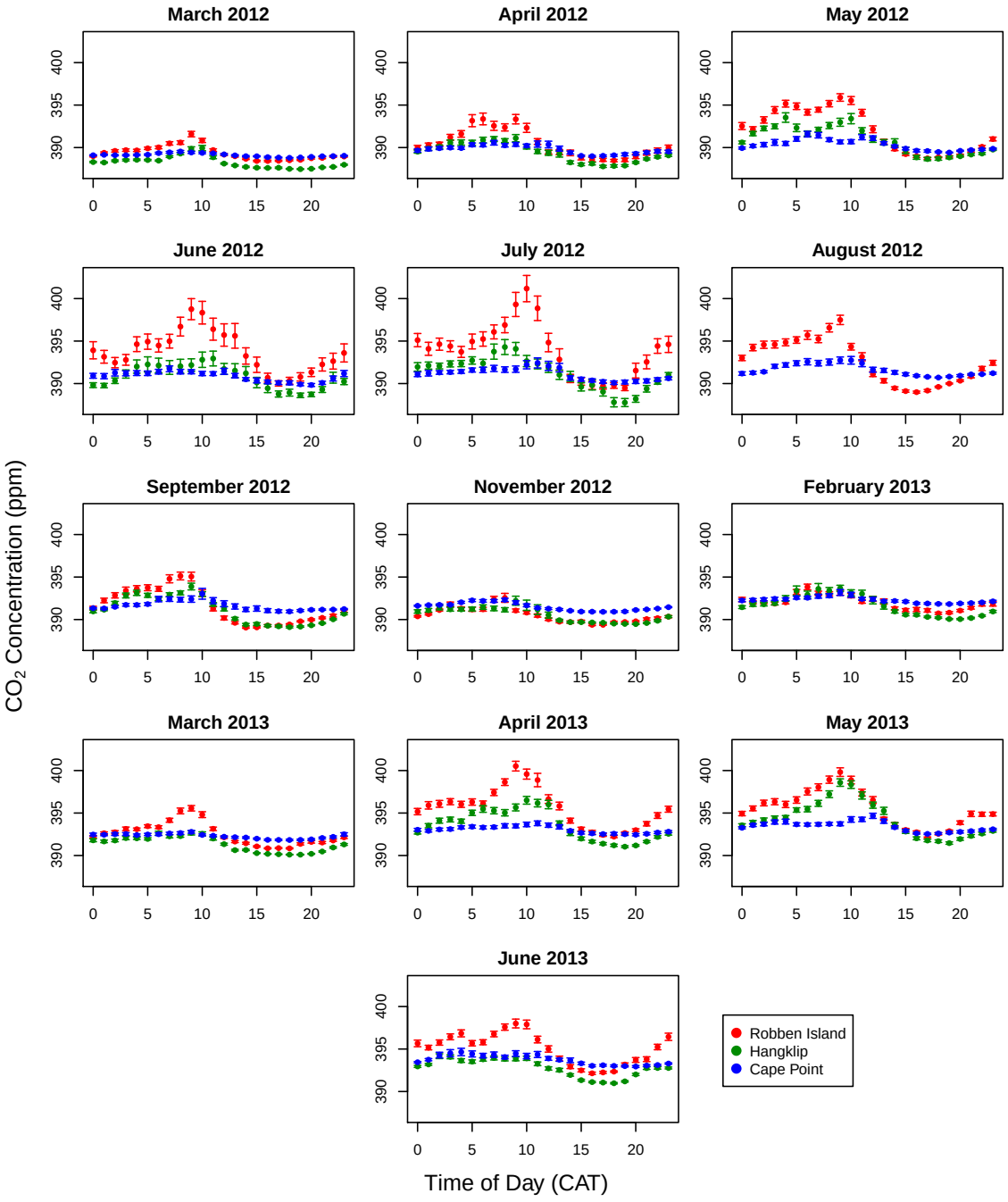

Figure S2. Diurnal cycle of the observed CO_2 concentrations (ppm) for each month and at each site with 95% confidence intervals, where the standard error is calculated over all measurements available for that hour of the day during that particular month. Cape Point is the generally flat diurnal cycle in blue, Robben Island with the generally larger daytime CO_2 concentrations in red, and Hangklip with the generally lower afternoon CO_2 concentrations in black.

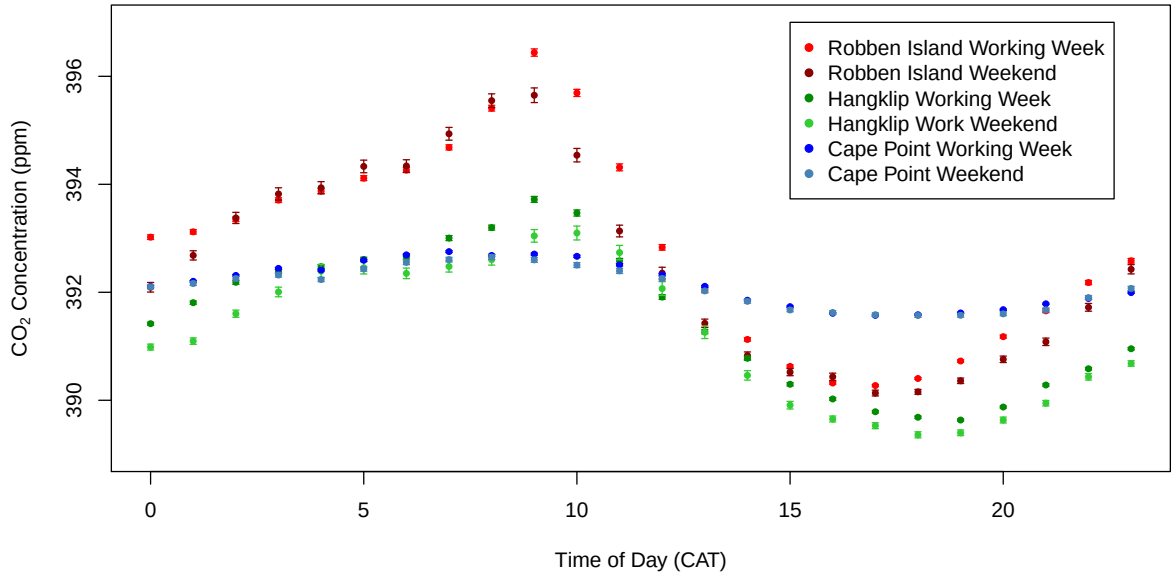

Figure S3. Diurnal cycle of the observed CO_2 concentrations (ppm) over the full measurement period from March 2012 until June 2013 at each site with 95% confidence intervals, where the standard error is calculated over all measurements available for that hour of the day during the entire measurement period, separated by site (Cape Point - blue and light blue, Robben Island - red and dark red, Hangklip - black and grey) and by working week (brighter colour) and weekend (duller colour).

The mean diurnal cycle over the whole measurement period is presented in Figure S3, separated by site and by working week and weekend. The background site, Cape Point, shows no discernible difference between the mean concentrations over the week and weekend, whereas Robben Island and Hangklip sites measure concentrations during the working week which tend to be larger across most of the day. Both the early morning and afternoon means show a clear tendency for these sites to have larger concentrations during the working week compared with the same time of day over the weekend, which can only be due to anthropogenic influences. This supports the separation of fossil fuel fluxes into working week and weekend contributions.

Table S2. The number of days with available CO_2 measurement data for each month (out of a possible four week period considered) and overall percentage available data out of 16 four-week periods for each site.

Site	Year / Month																Overall Percentage
	2012										2013						
	3	4	5	6	7	8	9	10	11	12	1	2	3	4	5	6	
Robben Island	28	21	28	14	14	28	28	0	14	0	0	21	28	28	28	28	68.75
Hangklip	28	21	28	14	14	0	28	0	14	0	0	21	28	28	28	28	62.50
Combined	56	42	56	28	28	28	56	0	28	0	0	42	56	56	56	56	65.63

Table S2 provides the measured CO_2 concentration availability at each site. Robben Island had slightly higher data availability compared with Hangklip, with a 65.6% data availability overall for the sixteen month measurement campaign. Each site was equipped with a Hauwei USB modem connected to a 3G network, and were set to submit data to an email address on a regular basis. Through these emails or through connecting remotely to the instruments, instrumentation problems could be detected. Most of the down-time at the sites was attributed to either pump failure, or occasionally the instrument software had failed and there was no available person to restart the instrument due to limited access to these sites. Robben Island lighthouse is manned, and therefore it was possible to request the lighthouse keeper to restart the instrument when frozen, but more regular than expected pump problems required visits to the site to replace the offending device. This entailed making arrangements for unplanned voyages to Robben Island, which could take some time to arrange. Hangklip is unmanned, and the site has strict access control, therefore problems at this site tended to take slightly longer to remedy. The final four months considered in this study had the best continuity of data availability.

1.2 Model Assessment

To determine if the prescribed prior covariance parameters were consistent with the model assumptions, the sum of the squared normalised residuals was compared against the χ^2 distribution. For most months the standardised statistic was close to one, but in the case of June and July 2012, this statistic was above 2. We did not scale the variances independently for each month, and therefore the single scaling factor of 2 for the prior flux variances was not large enough for all months. The statistic remained below 2.5 for all months, and had a minimum of 0.68 for the month of November 2012. The mean of the statistic over all months was 1.48. A subsequent study will assess an alternative approach to determine prior flux uncertainties, which would guarantee compliance of the sum of the squared normalised residuals to follow the χ^2 distribution.

Table S3. Sum of the squared normalised residuals for each month, which should approximate a χ^2 distribution with one degree of freedom.

Month	χ^2 statistic	Percentage available data
Mar2012	1.006	100%
Apr2012	1.089	75%
May2012	1.959	100%
Jun2012	2.473	50%
Jul2012	2.170	50%
Aug2012	1.586	50%
Sep2012	1.028	100%
Nov2012	0.678	50%
Feb2012	0.938	75%
Mar2013	1.048	100%
Apr2013	1.776	100%
May2013	1.829	100%
Jun2013	1.706	100%

1.3 Modelled Wind

Figure S4 provides the average wind speed and direction for the domain for each month, as modelled by CCAM. The plots were created using the R package rasterVis (Lamigueiro, 2016).

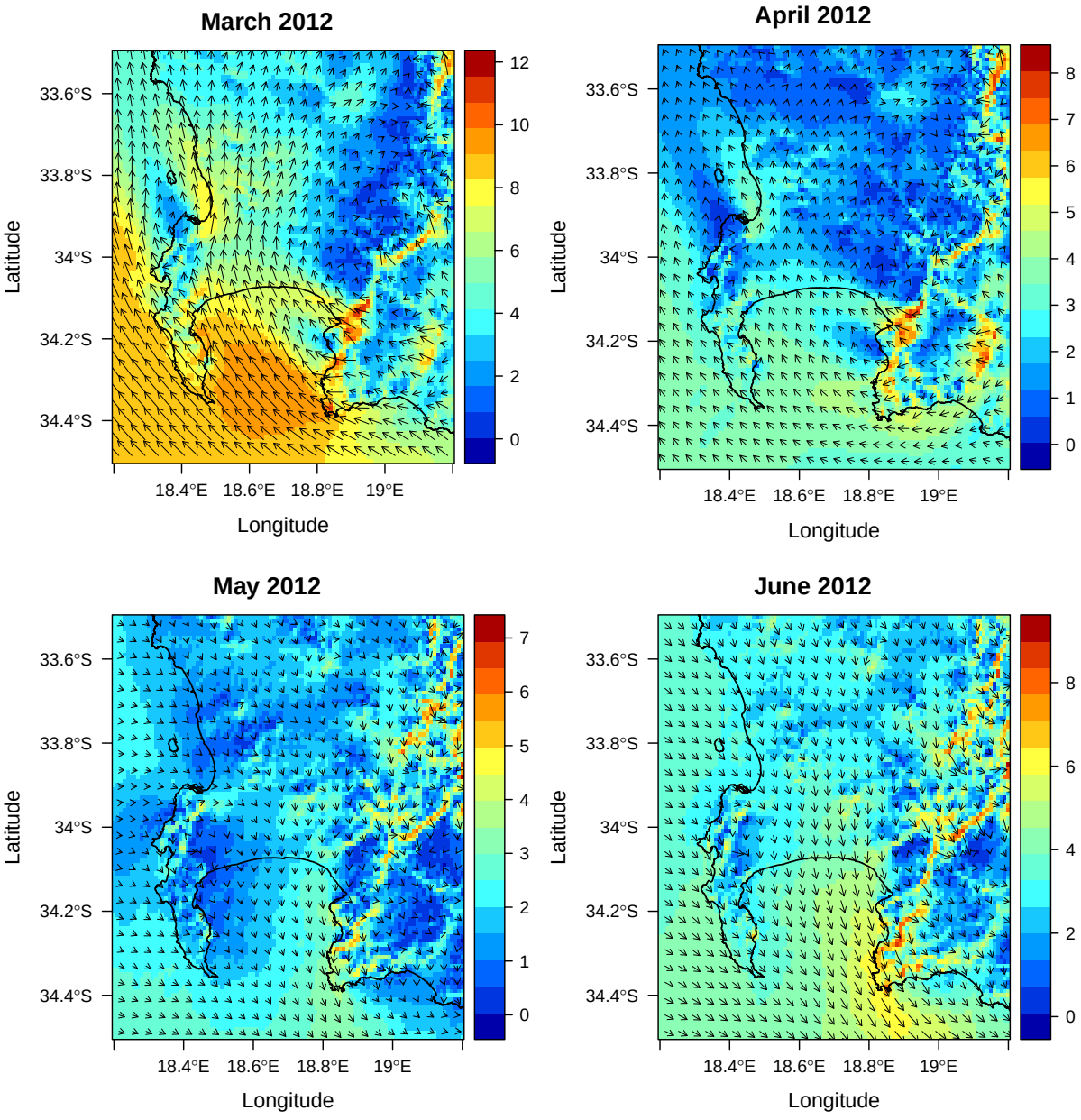

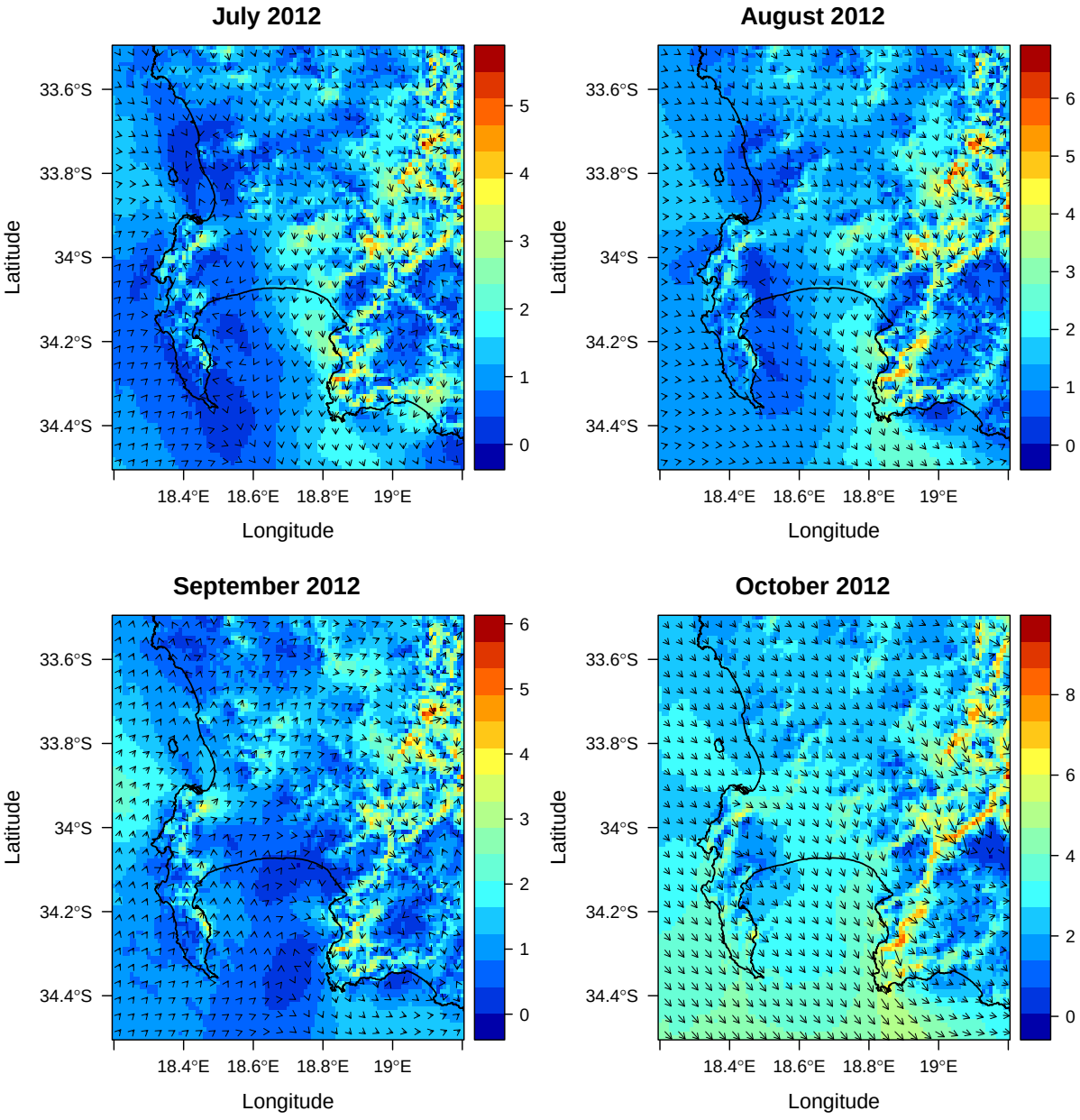
July 2012
August 2012
September 2012
October 2012
Latitude
Longitude
33.6°S
33.8°S
34°S
34.2°S
34.4°S
18.4°E
18.6°E
18.8°E
19°E

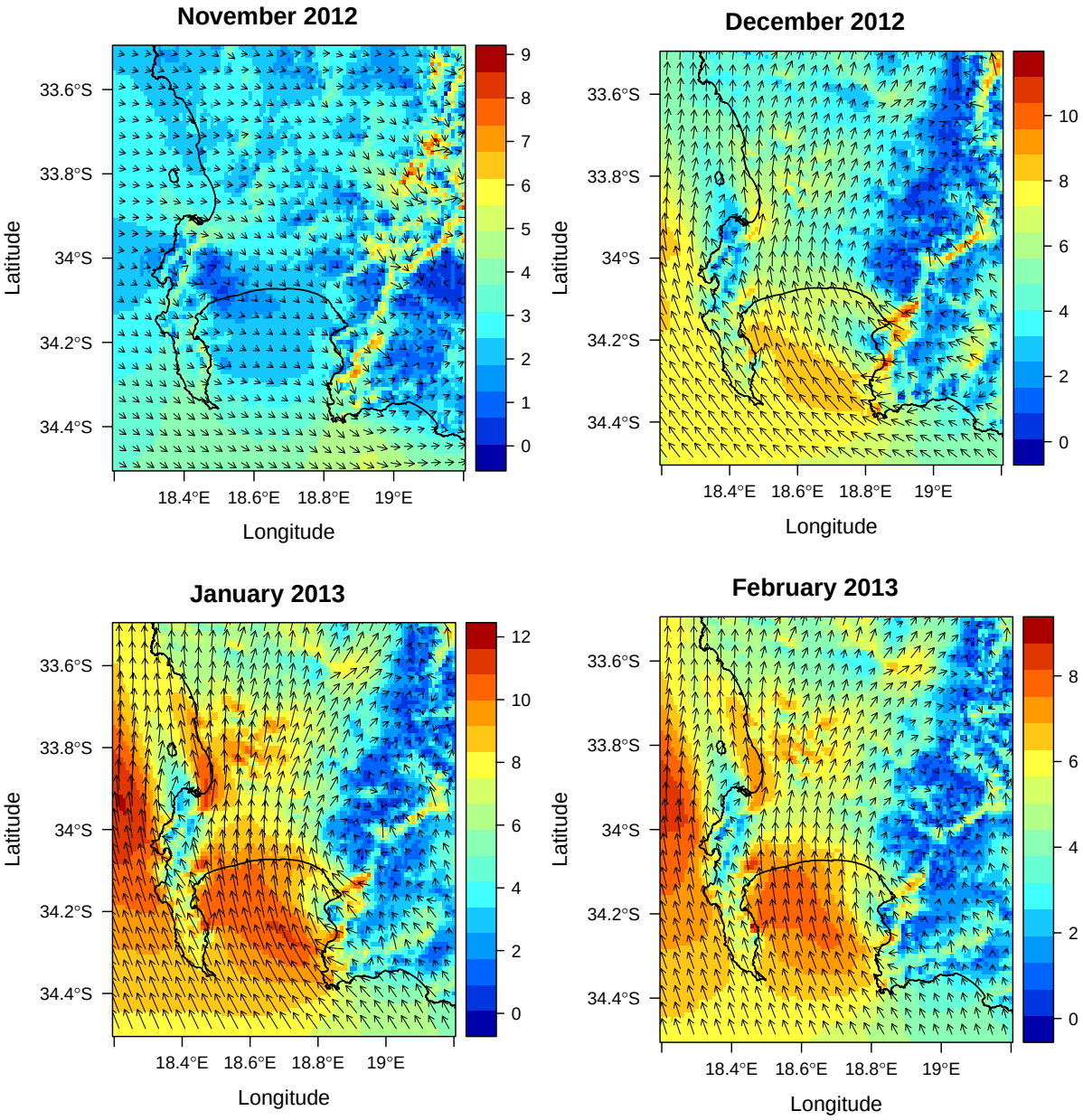
November 2012
December 2012
January 2013
February 2013
Latitude
Longitude
33.6°S
33.8°S
34°S
34.2°S
34.4°S
18.4°E
18.6°E
18.8°E
19°E

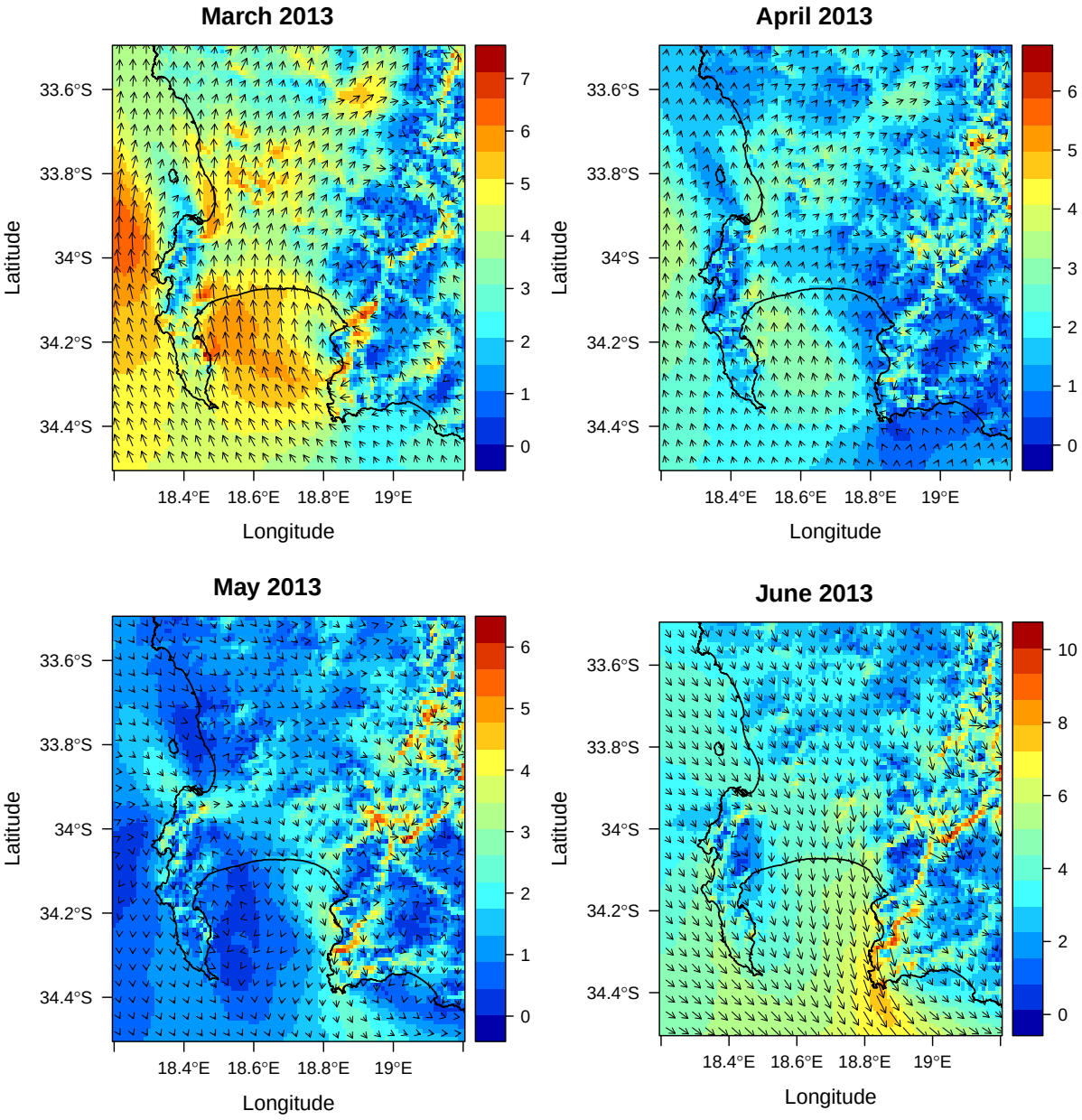

Figure S4. Mean modelled wind speed and direction in the Cape Town domain for each month. The colourbar represents the mean wind speed (m/s).

1.4 Modelled Concentrations

The time series for the modelled concentrations is discussed in Section 3.1 of the main paper.

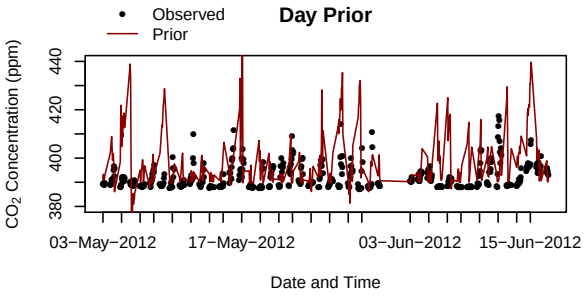
Observed
Prior
Day Prior
CO2 Concentration (ppm)
380
400
420
440
03−May−2012
17−May−2012
03−Jun−2012
15−Jun−2012
Date and Time

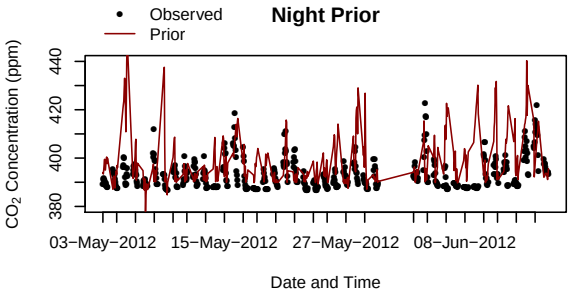
Observed
Prior
Night Prior
CO2 Concentration (ppm)
380
400
420
440
03−May−2012
15−May−2012
27−May−2012
08−Jun−2012
Date and Time

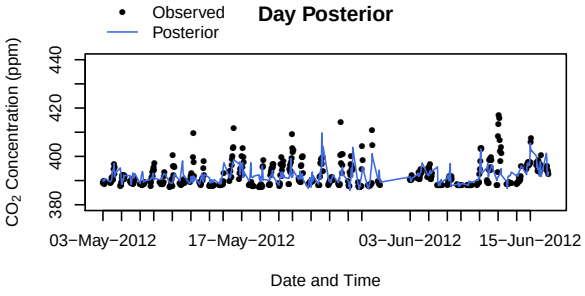
Observed
Posterior
Day Posterior
CO2 Concentration (ppm)
380
400
420
440
03−May−2012
17−May−2012
03−Jun−2012
15−Jun−2012
Date and Time

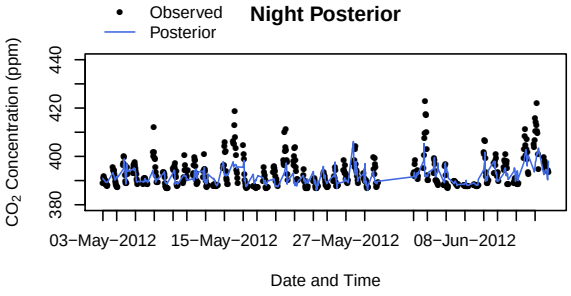
Observed
Posterior
Night Posterior
CO2 Concentration (ppm)
380
400
420
440
03−May−2012
15−May−2012
27−May−2012
08−Jun−2012
Date and Time

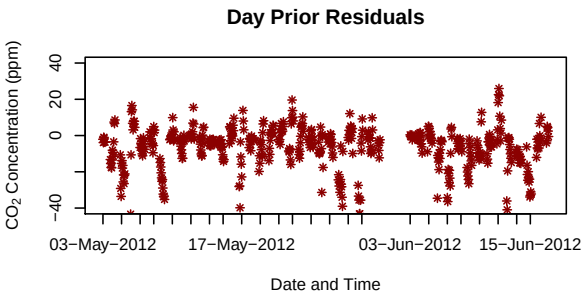
Day Prior Residuals
CO2 Concentration (ppm)
−40
0
20
40
03−May−2012
17−May−2012
03−Jun−2012
15−Jun−2012
Date and Time

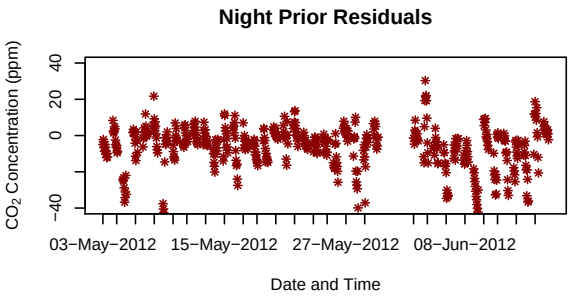
Night Prior Residuals
CO2 Concentration (ppm)
−40
0
20
40
03−May−2012
15−May−2012
27−May−2012
08−Jun−2012
Date and Time

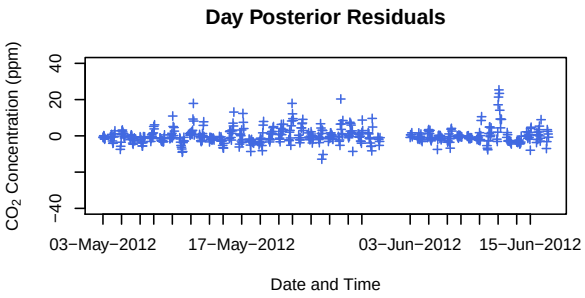
Day Posterior Residuals
CO2 Concentration (ppm)
−40
0
20
40
03−May−2012
17−May−2012
03−Jun−2012
15−Jun−2012
Date and Time

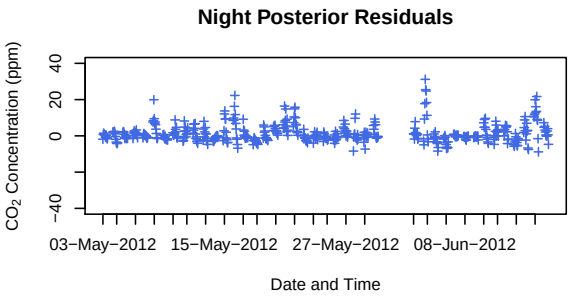
Night Posterior Residuals
CO2 Concentration (ppm)
−40
0
20
40
03−May−2012
15−May−2012
27−May−2012
08−Jun−2012
Date and Time

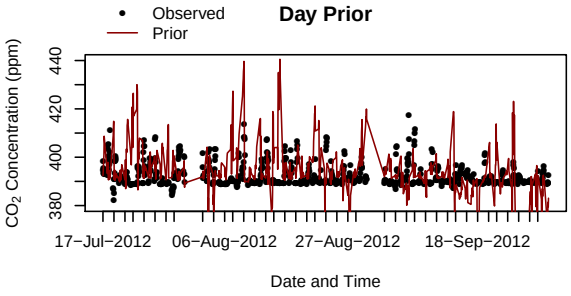
Observed
Prior
Day Prior
CO2 Concentration (ppm)
380
400
420
440
17−Jul−2012
06−Aug−2012
27−Aug−2012
18−Sep−2012
Date and Time

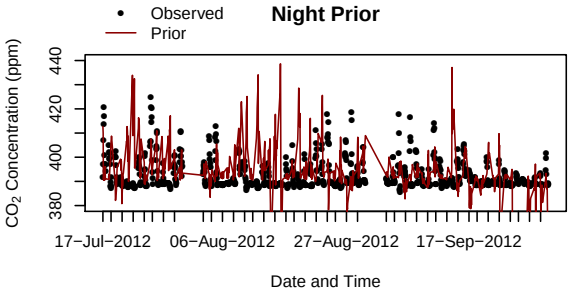
Observed
Prior
Night Prior
CO2 Concentration (ppm)
380
400
420
440
17−Jul−2012
06−Aug−2012
27−Aug−2012
17−Sep−2012
Date and Time

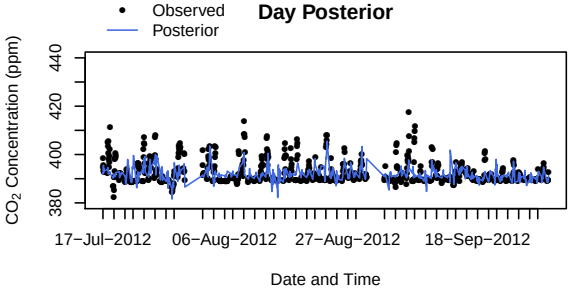
Observed
Posterior
Day Posterior
CO2 Concentration (ppm)
380
400
420
440
17−Jul−2012
06−Aug−2012
27−Aug−2012
18−Sep−2012
Date and Time

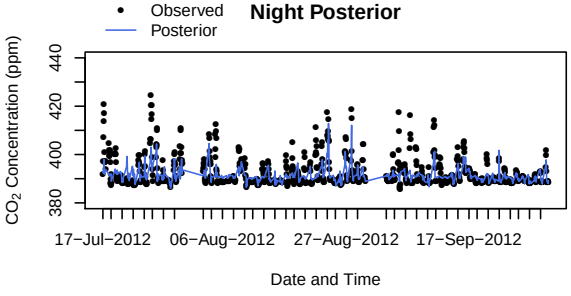
Observed
Posterior
Night Posterior
CO2 Concentration (ppm)
380
400
420
440
17−Jul−2012
06−Aug−2012
27−Aug−2012
17−Sep−2012
Date and Time

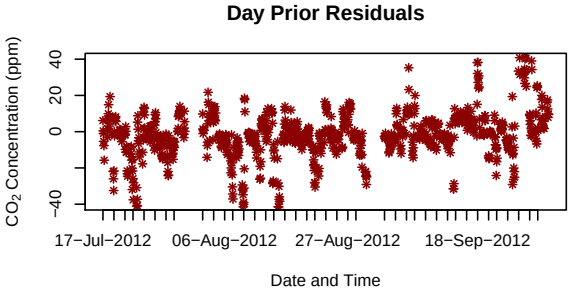
Day Prior Residuals
CO2 Concentration (ppm)
−40
0
20
40
17−Jul−2012
06−Aug−2012
27−Aug−2012
18−Sep−2012
Date and Time

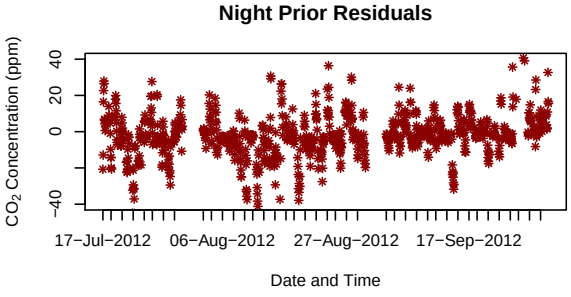
Night Prior Residuals
CO2 Concentration (ppm)
−40
0
20
40
17−Jul−2012
06−Aug−2012
27−Aug−2012
17−Sep−2012
Date and Time

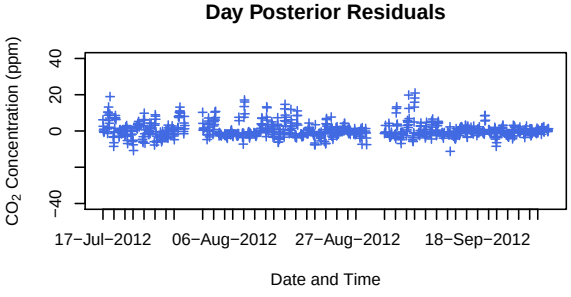
Day Posterior Residuals
CO2 Concentration (ppm)
−40
0
20
40
17−Jul−2012
06−Aug−2012
27−Aug−2012
18−Sep−2012
Date and Time

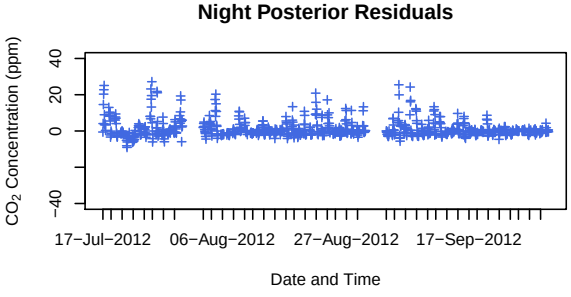
Night Posterior Residuals
CO2 Concentration (ppm)
−40
0
20
40
17−Jul−2012
06−Aug−2012
27−Aug−2012
17−Sep−2012
Date and Time

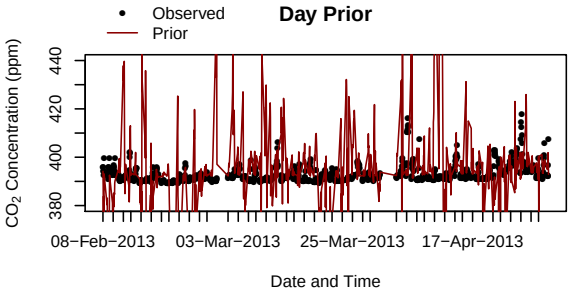
Observed
Prior
Day Prior
CO2 Concentration (ppm)
380
400
420
440
08−Feb−2013
03−Mar−2013
25−Mar−2013
17−Apr−2013
Date and Time

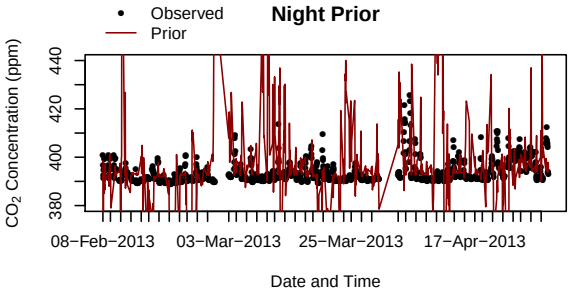
Observed
Prior
Night Prior
CO2 Concentration (ppm)
380
400
420
440
08−Feb−2013
03−Mar−2013
25−Mar−2013
17−Apr−2013
Date and Time

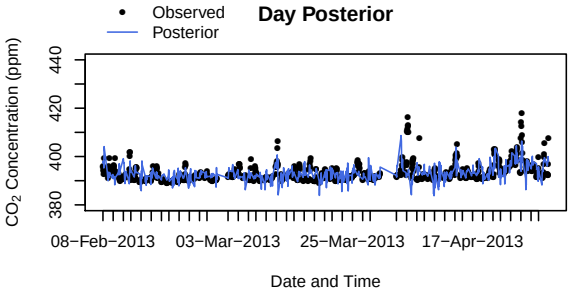
Observed
Posterior
Day Posterior
CO2 Concentration (ppm)
380
400
420
440
08−Feb−2013
03−Mar−2013
25−Mar−2013
17−Apr−2013
Date and Time

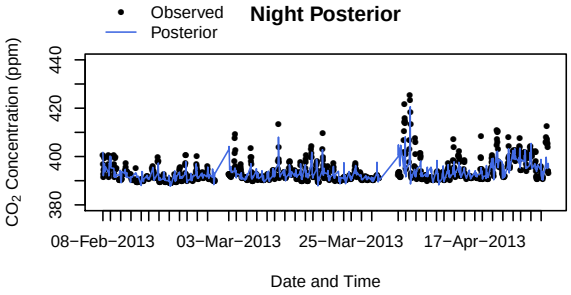
Observed
Posterior
Night Posterior
CO2 Concentration (ppm)
380
400
420
440
08−Feb−2013
03−Mar−2013
25−Mar−2013
17−Apr−2013
Date and Time

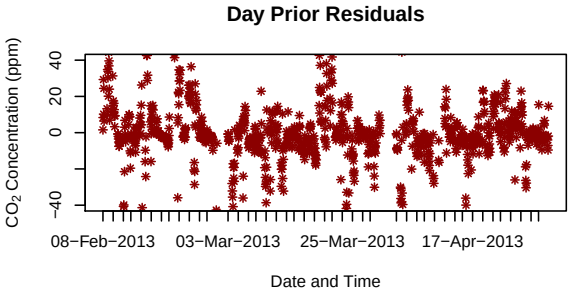
Day Prior Residuals
CO2 Concentration (ppm)
−40
0
20
40
08−Feb−2013
03−Mar−2013
25−Mar−2013
17−Apr−2013
Date and Time

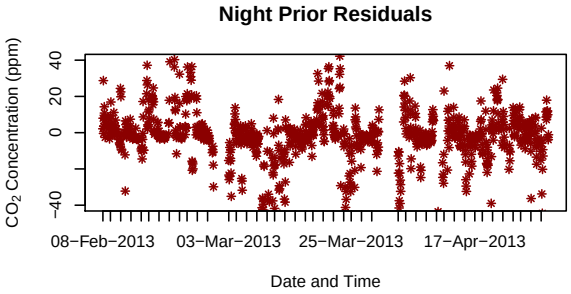
Night Prior Residuals
CO2 Concentration (ppm)
−40
0
20
40
08−Feb−2013
03−Mar−2013
25−Mar−2013
17−Apr−2013
Date and Time

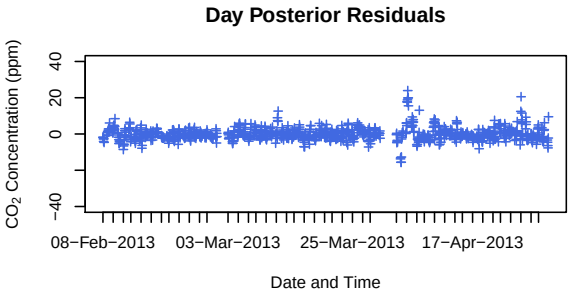
Day Posterior Residuals
CO2 Concentration (ppm)
−40
0
20
40
08−Feb−2013
03−Mar−2013
25−Mar−2013
17−Apr−2013
Date and Time

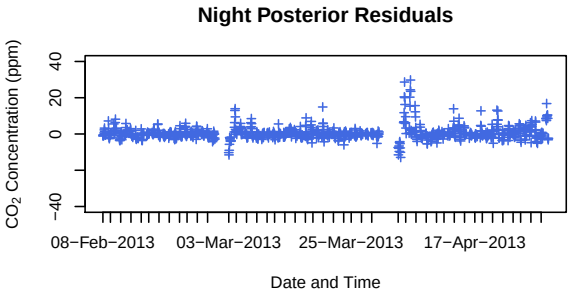
Night Posterior Residuals
CO2 Concentration (ppm)
−40
0
20
40
08−Feb−2013
03−Mar−2013
25−Mar−2013
17−Apr−2013
Date and Time

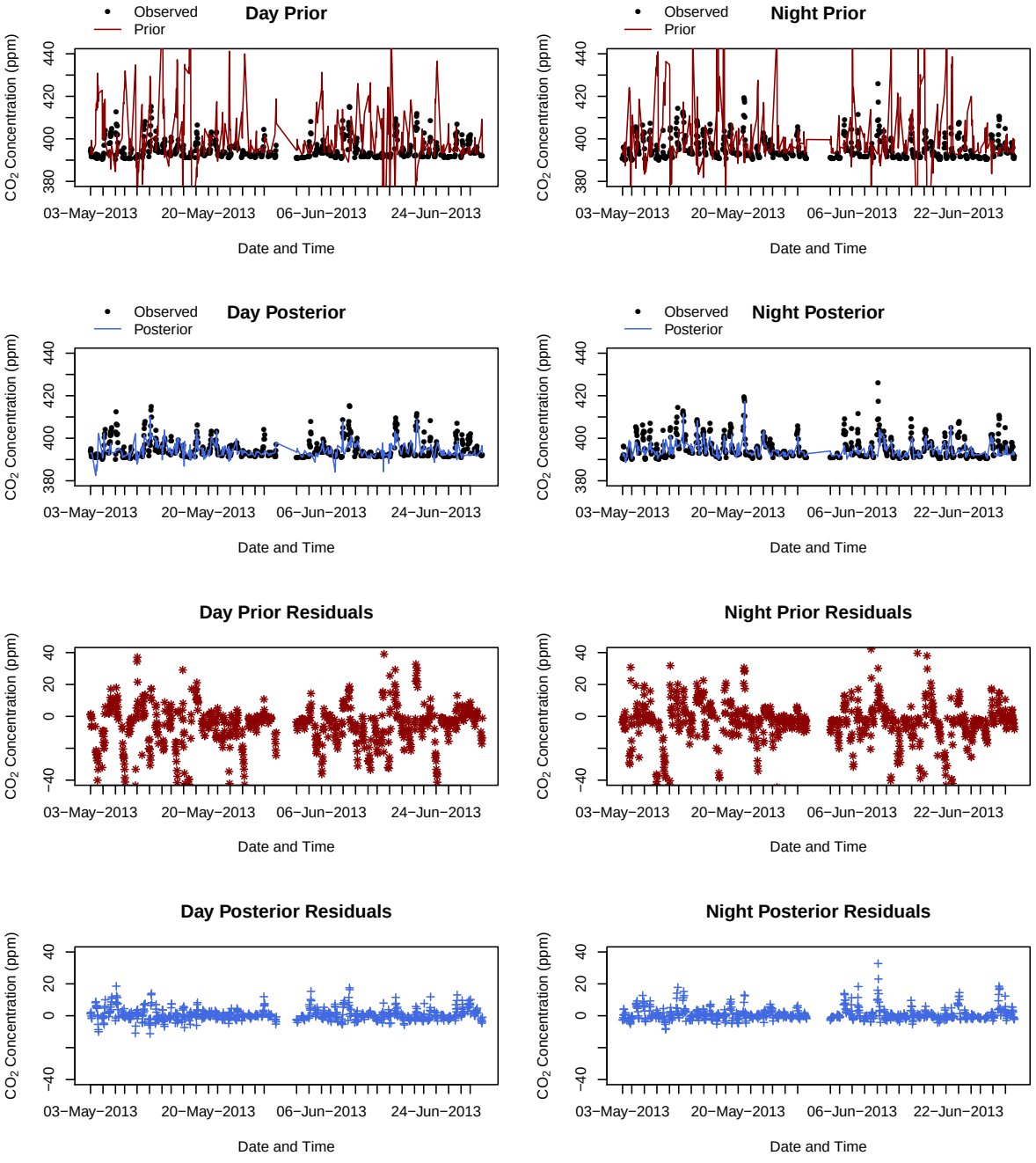

Figure S5. The top 4 panels provide a time series of the observed, prior and posterior modelled concentrations at the Robben Island site. The time series is separated into day and night-time periods. The residuals between the modelled and observed concentrations, defined as the difference between the observed and modelled concentrations, are provided in the lower panel 4 panels. The first 2 months are presented in the main paper in section 3.1.

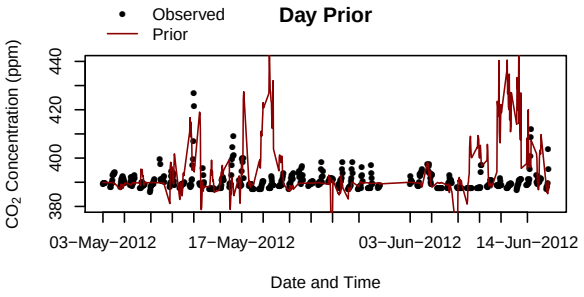
Observed
Prior
Day Prior
CO2 Concentration (ppm)
380
400
420
440
03−May−2012
17−May−2012
03−Jun−2012
14−Jun−2012
Date and Time

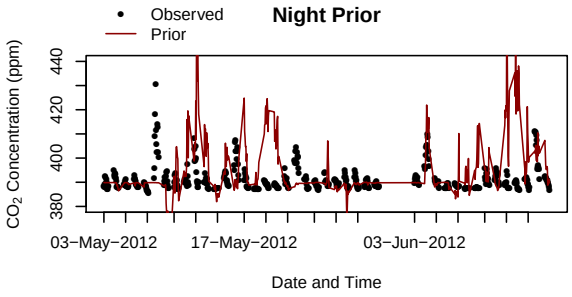
Observed
Prior
Night Prior
CO2 Concentration (ppm)
380
400
420
440
03−May−2012
17−May−2012
03−Jun−2012
Date and Time

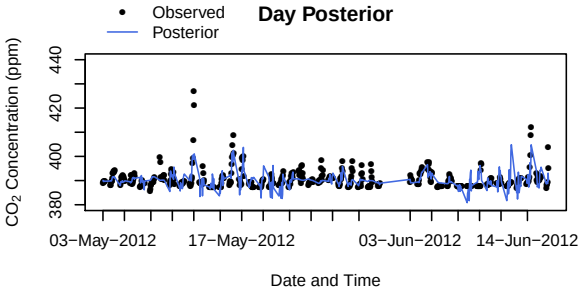
Observed
Posterior
Day Posterior
CO2 Concentration (ppm)
380
400
420
440
03−May−2012
17−May−2012
03−Jun−2012
14−Jun−2012
Date and Time

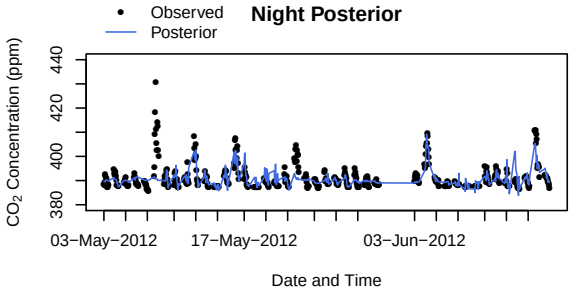
Observed
Posterior
Night Posterior
CO2 Concentration (ppm)
380
400
420
440
03−May−2012
17−May−2012
03−Jun−2012
Date and Time

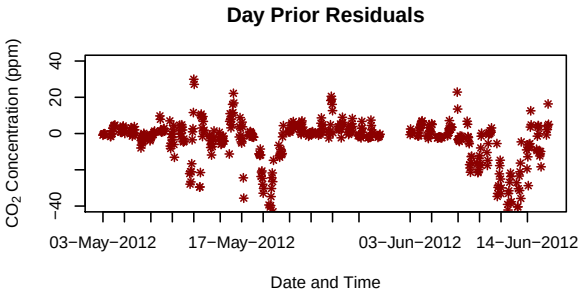
Day Prior Residuals
CO2 Concentration (ppm)
−40
0
20
40
03−May−2012
17−May−2012
03−Jun−2012
14−Jun−2012
Date and Time

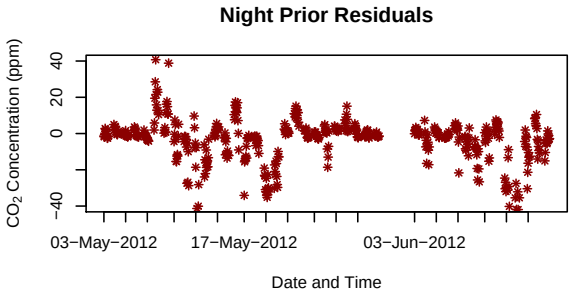
Night Prior Residuals
CO2 Concentration (ppm)
−40
0
20
40
03−May−2012
17−May−2012
03−Jun−2012
Date and Time

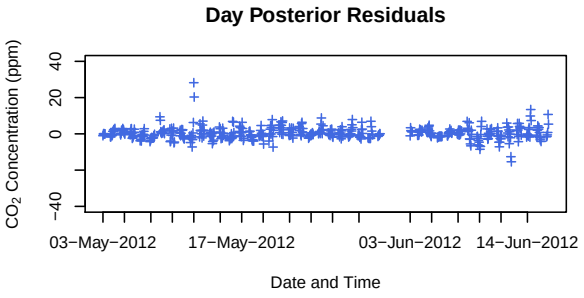
Day Posterior Residuals
CO2 Concentration (ppm)
−40
0
20
40
03−May−2012
17−May−2012
03−Jun−2012
14−Jun−2012
Date and Time

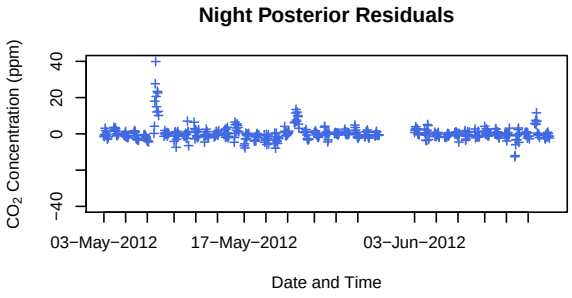
Night Posterior Residuals
CO2 Concentration (ppm)
−40
0
20
40
03−May−2012
17−May−2012
03−Jun−2012
Date and Time

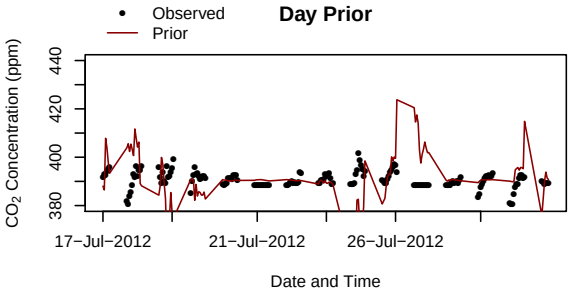
Observed
Prior
Day Prior
CO2 Concentration (ppm)
380
400
420
440
17−Jul−2012
21−Jul−2012
26−Jul−2012
Date and Time

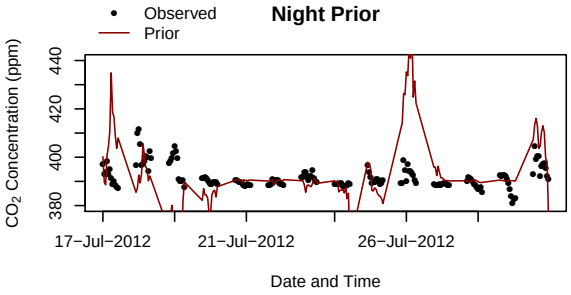
Observed
Prior
Night Prior
CO2 Concentration (ppm)
380
400
420
440
17−Jul−2012
21−Jul−2012
26−Jul−2012
Date and Time

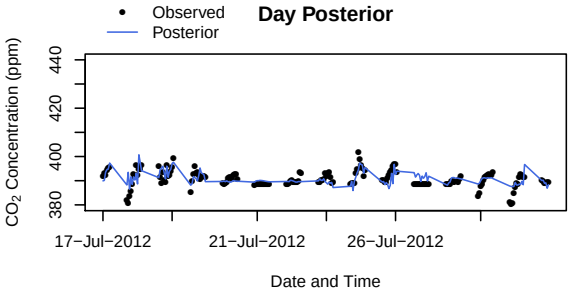
Observed
Posterior
Day Posterior
CO2 Concentration (ppm)
380
400
420
440
17−Jul−2012
21−Jul−2012
26−Jul−2012
Date and Time

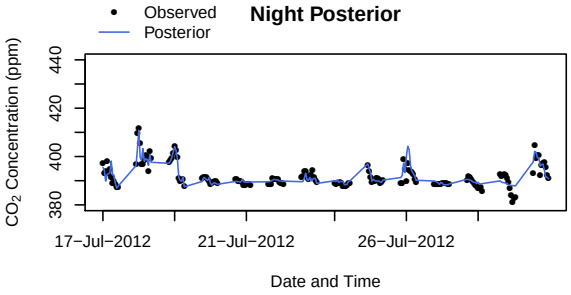
Observed
Posterior
Night Posterior
CO2 Concentration (ppm)
380
400
420
440
17−Jul−2012
21−Jul−2012
26−Jul−2012
Date and Time

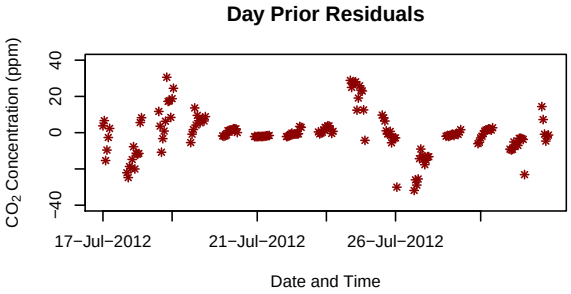
Day Prior Residuals
CO2 Concentration (ppm)
−40
0
20
40
17−Jul−2012
21−Jul−2012
26−Jul−2012
Date and Time

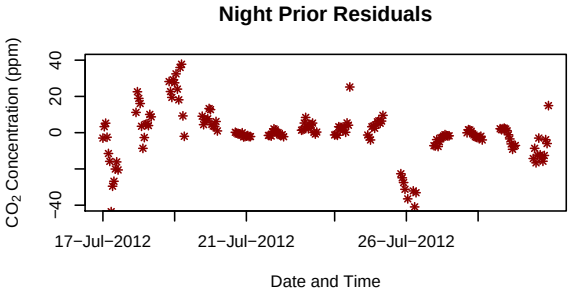
Night Prior Residuals
CO2 Concentration (ppm)
−40
0
20
40
17−Jul−2012
21−Jul−2012
26−Jul−2012
Date and Time

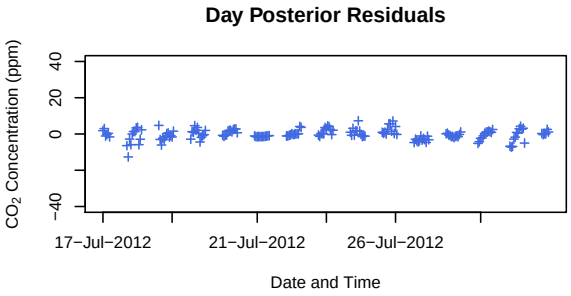
Day Posterior Residuals
CO2 Concentration (ppm)
−40
0
20
40
17−Jul−2012
21−Jul−2012
26−Jul−2012
Date and Time

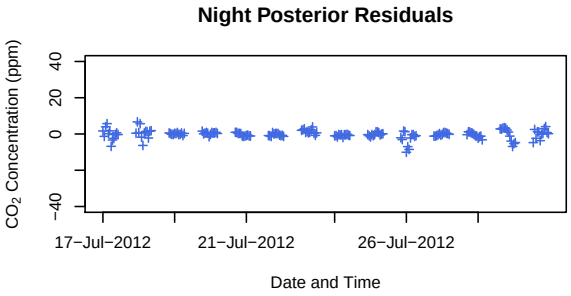
Night Posterior Residuals
CO2 Concentration (ppm)
−40
0
20
40
17−Jul−2012
21−Jul−2012
26−Jul−2012
Date and Time

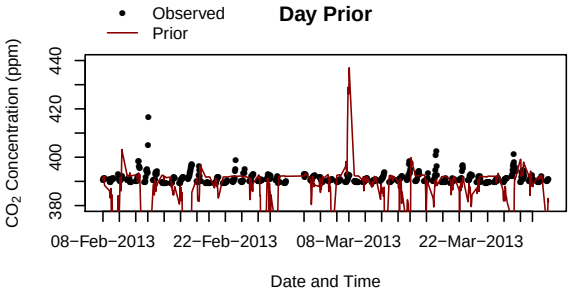
Observed
Prior
Day Prior
CO2 Concentration (ppm)
380
400
420
440
08−Feb−2013
22−Feb−2013
08−Mar−2013
22−Mar−2013
Date and Time

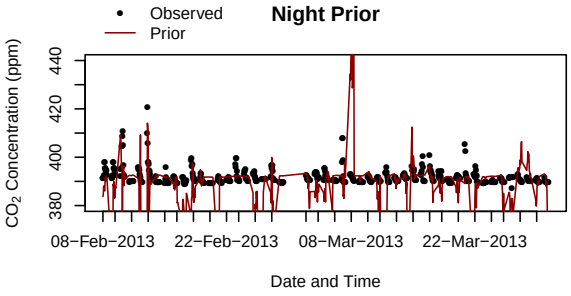
Observed
Prior
Night Prior
CO2 Concentration (ppm)
380
400
420
440
08−Feb−2013
22−Feb−2013
08−Mar−2013
22−Mar−2013
Date and Time

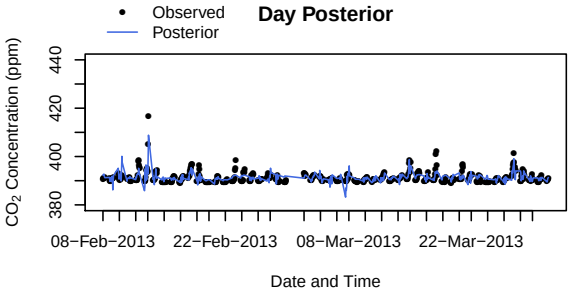
Observed
Posterior
Day Posterior
CO2 Concentration (ppm)
380
400
420
440
08−Feb−2013
22−Feb−2013
08−Mar−2013
22−Mar−2013
Date and Time

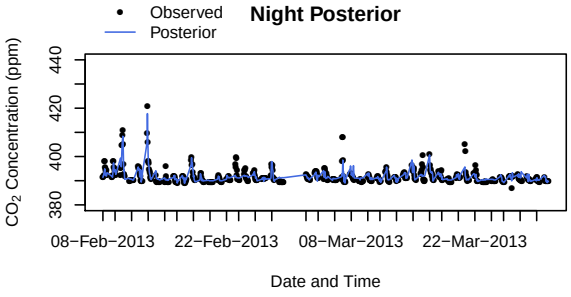
Observed
Posterior
Night Posterior
CO2 Concentration (ppm)
380
400
420
440
08−Feb−2013
22−Feb−2013
08−Mar−2013
22−Mar−2013
Date and Time

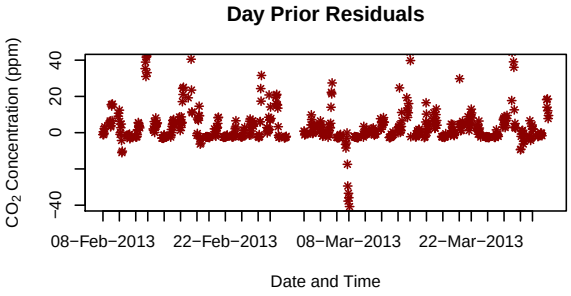
Day Prior Residuals
CO2 Concentration (ppm)
−40
0
20
40
08−Feb−2013
22−Feb−2013
08−Mar−2013
22−Mar−2013
Date and Time

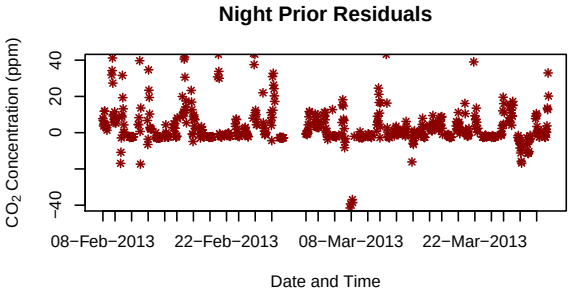
Night Prior Residuals
CO2 Concentration (ppm)
−40
0
20
40
08−Feb−2013
22−Feb−2013
08−Mar−2013
22−Mar−2013
Date and Time

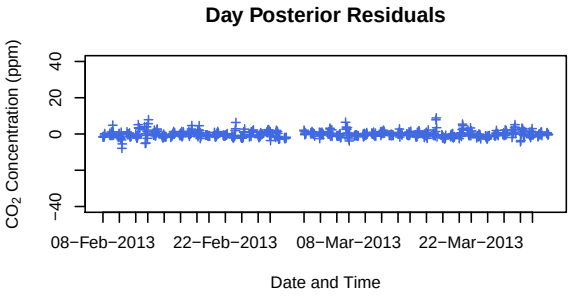
Day Posterior Residuals
CO2 Concentration (ppm)
−40
0
20
40
08−Feb−2013
22−Feb−2013
08−Mar−2013
22−Mar−2013
Date and Time

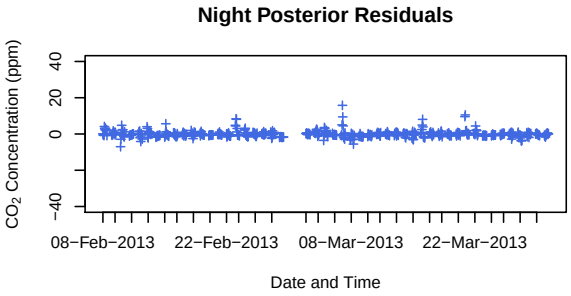
Night Posterior Residuals
CO2 Concentration (ppm)
−40
0
20
40
08−Feb−2013
22−Feb−2013
08−Mar−2013
22−Mar−2013
Date and Time

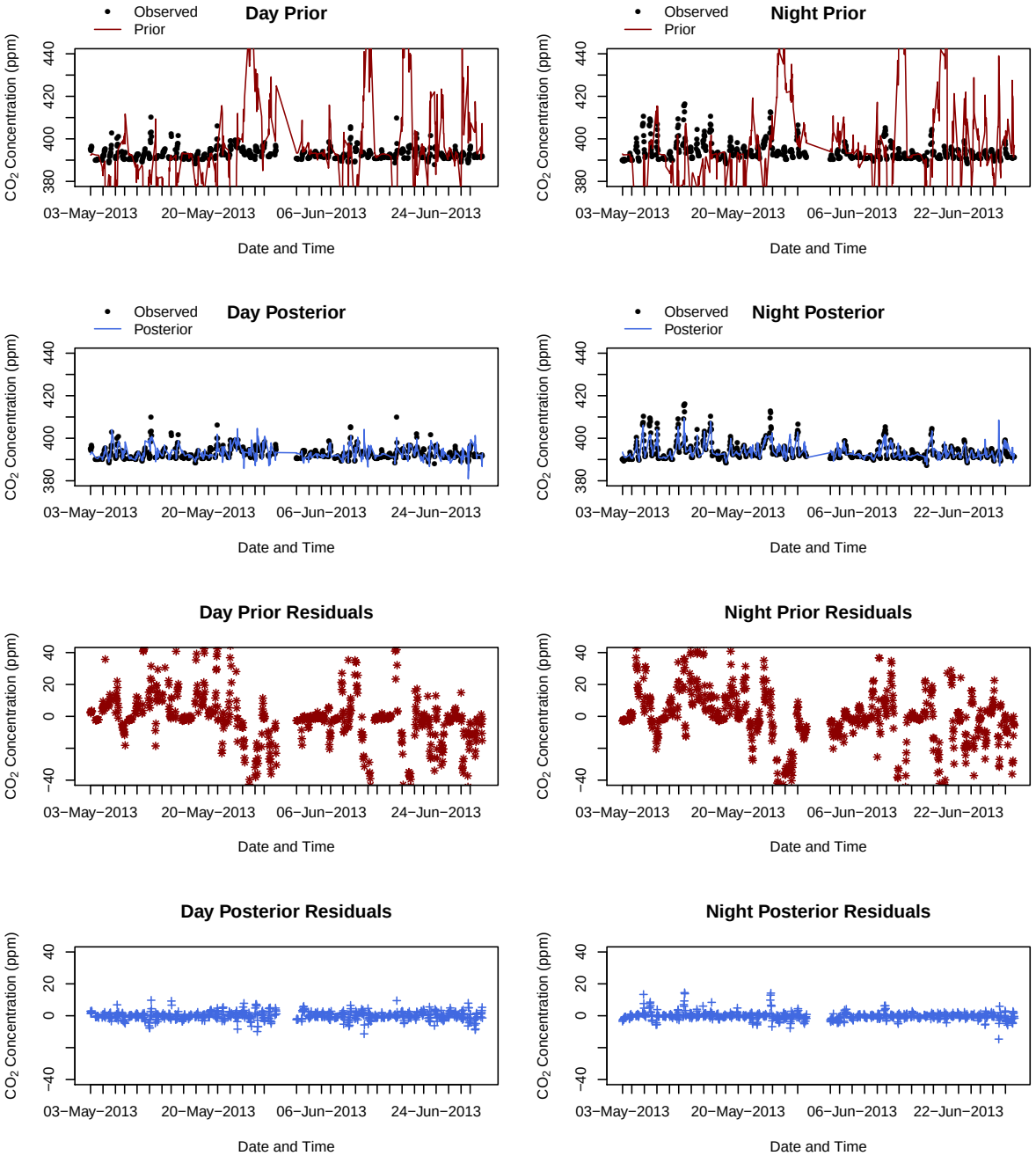

Figure S6. The top 4 panels provide a time series of the observed, prior and posterior modelled concentrations at the Hangklip site. The time series is separated into day and night-time periods. The residuals between the modelled and observed concentrations, defined as the difference between the observed and modelled concentrations, are provided in the lower panel 4 panels. The first 2 months are presented in the main paper in section 3.1.

1.5 Diurnal Cycle

The observed, prior and posterior modelled diurnal cycle, separated into working week and weekend CO_2 concentrations, are provided for each site and for each month in Figures S7 and S8. For all months, the diurnal cycle of the posterior modelled concentrations is relatively flat in comparison with the observed diurnal cycle, and usually sits at a higher mean level in the case of Robben Island, and at a lower mean level in the case of Hangklip. Compared with the prior modelled concentrations, the posterior diurnal cycle matches better with the observed concentrations in terms of the peaks and troughs of the cycle and in terms of the mean level of the concentrations at each hour, although the posterior cycle still appears relatively flat in comparison to the observed cycle.

April 2013 at the Robben Island site provides an example where the prior modelled concentrations had working week concentrations that were above those for the weekend during the early morning hours, whereas the observed concentrations showed the opposite situation. After the inversion, the posterior estimates had mean concentrations for the weekend that were above those for the working week during the early morning hours, matching better with the observed diurnal cycle.

Therefore the inversion does show an ability to improve estimates of the diurnal cycle, despite only separating the sources into day and night sources over a week period, and further separating the fossil fuel sources into weekend and week sources.

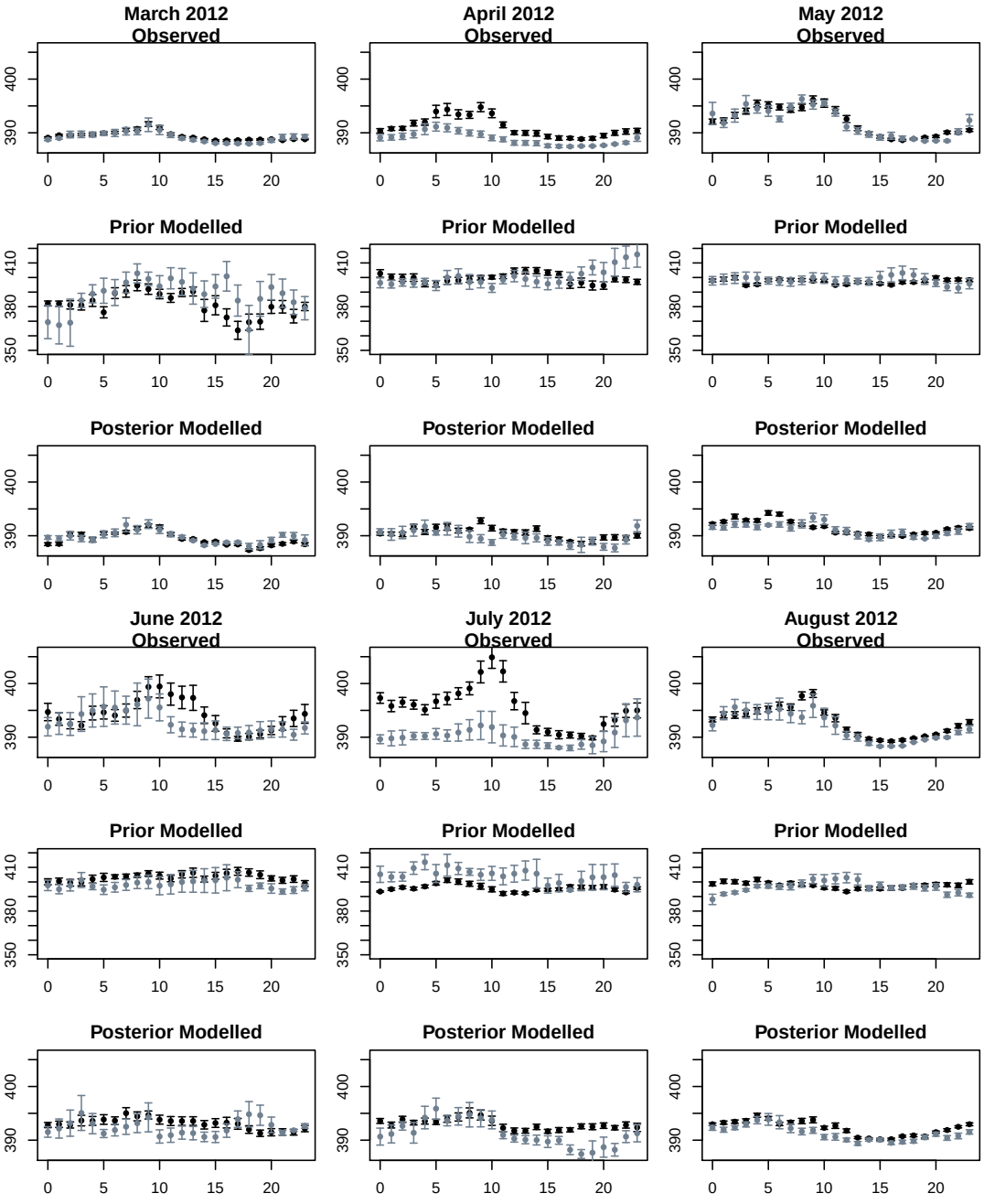
March 2012
Observed
April 2012
Observed
May 2012
Observed
Prior Modelled
Prior Modelled
Prior Modelled
Posterior Modelled
Posterior Modelled
Posterior Modelled
June 2012
Observed
July 2012
Observed
August 2012
Observed
Prior Modelled
Prior Modelled
Prior Modelled
Posterior Modelled
Posterior Modelled
Posterior Modelled

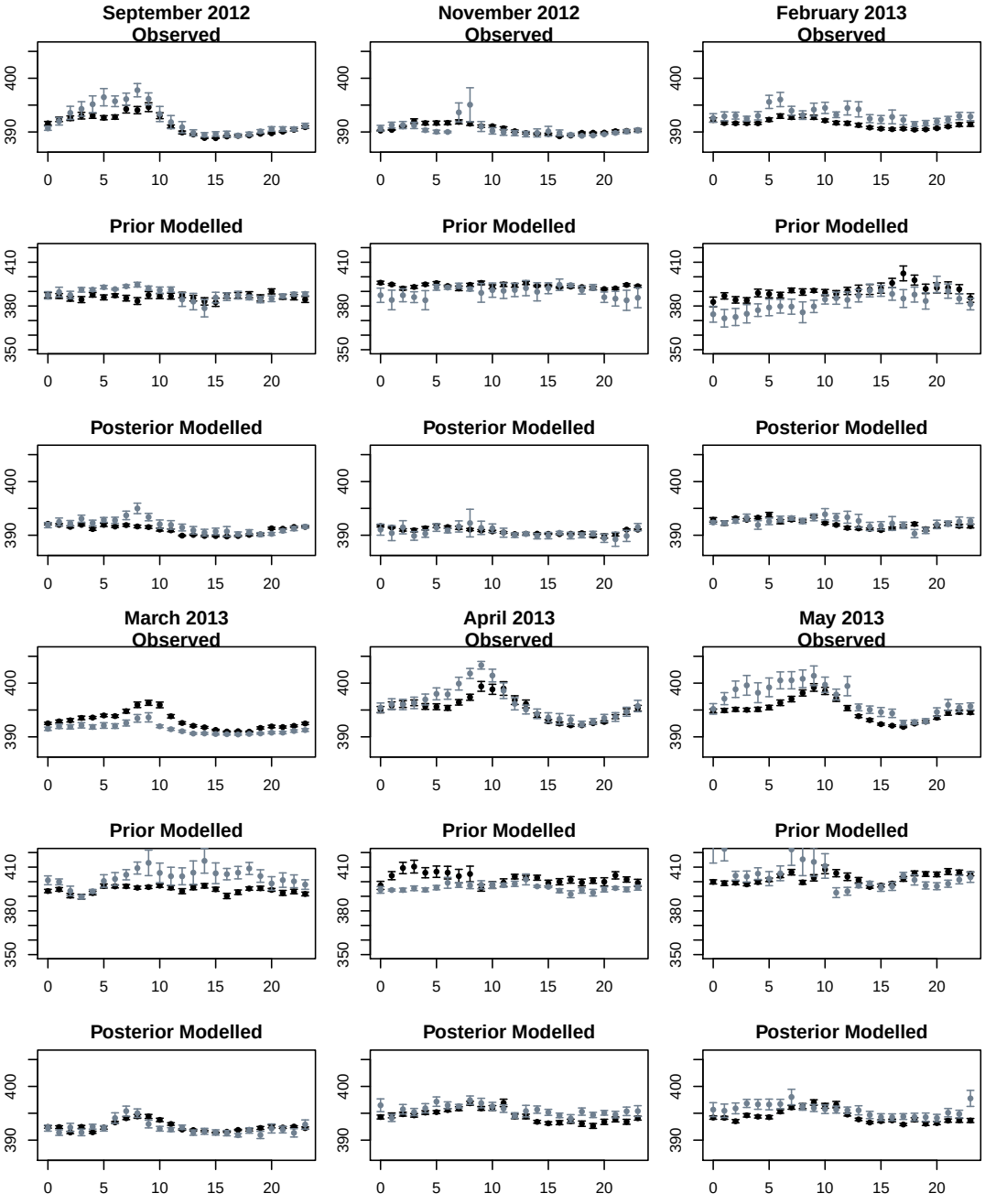
September 2012
Observed
November 2012
Observed
February 2013
Observed
Prior Modelled
Prior Modelled
Prior Modelled
Posterior Modelled
Posterior Modelled
Posterior Modelled
March 2013
Observed
April 2013
Observed
May 2013
Observed
Prior Modelled
Prior Modelled
Prior Modelled
Posterior Modelled
Posterior Modelled
Posterior Modelled

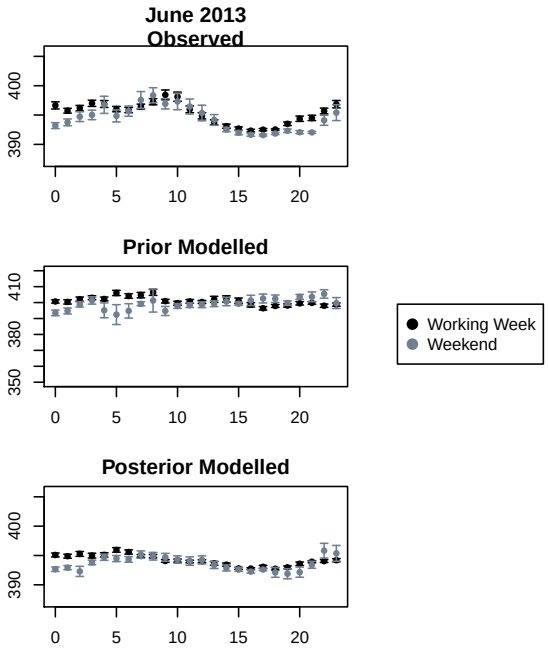

Figure S7. Diurnal cycle of the observed, prior modelled and posterior modelled CO_2 concentrations (ppm) at Robben Island, separated into working week (black) and weekend concentrations (grey), for each month with 95% confidence intervals, where the standard error is calculated over all measurements available for that hour of the day during that particular month.

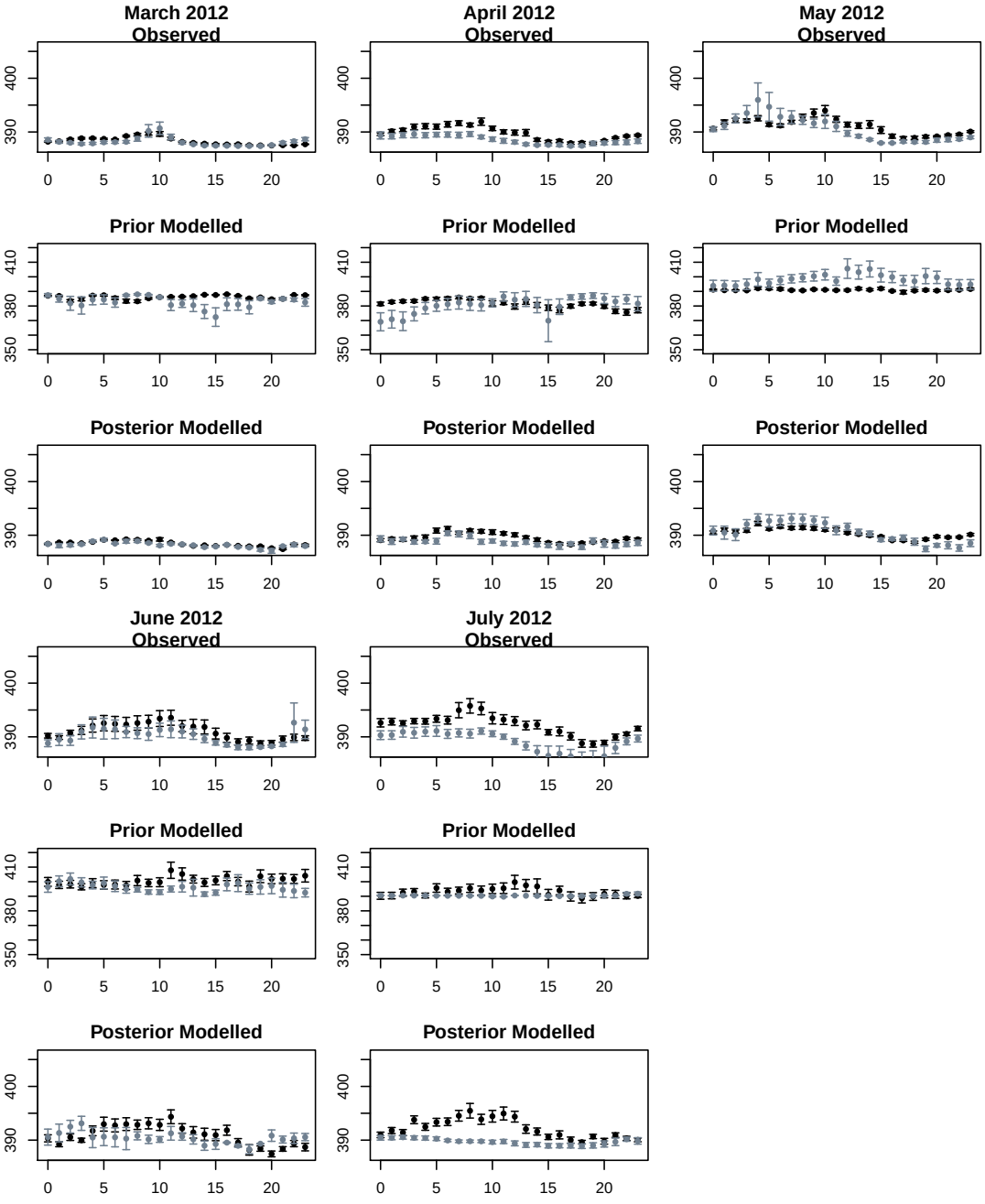
March 2012
Observed
April 2012
Observed
May 2012
Observed
Prior Modelled
Prior Modelled
Prior Modelled
Posterior Modelled
Posterior Modelled
Posterior Modelled
June 2012
Observed
July 2012
Observed
Prior Modelled
Prior Modelled
Posterior Modelled
Posterior Modelled

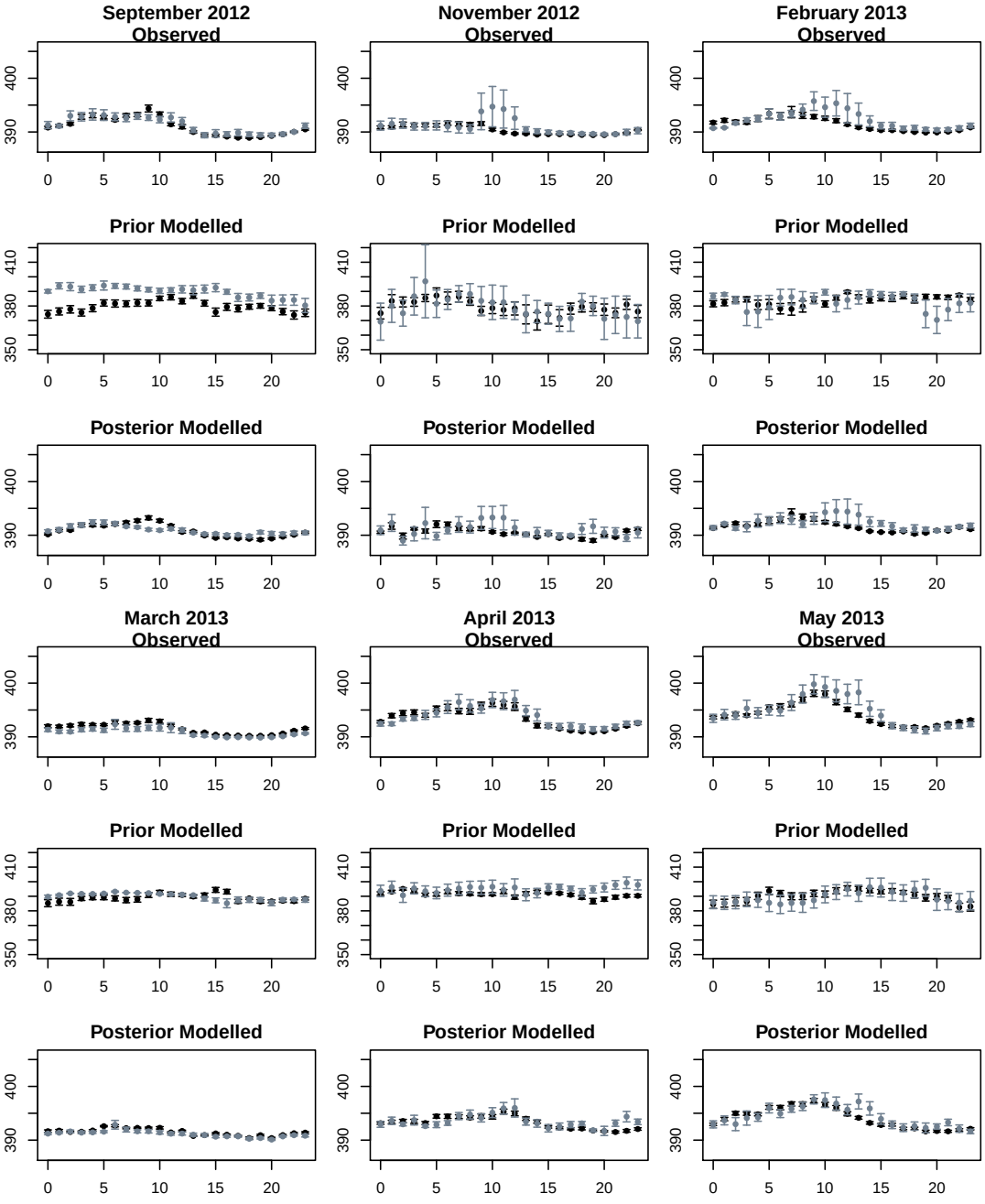
September 2012
Observed
November 2012
Observed
February 2013
Observed
Prior Modelled
Prior Modelled
Prior Modelled
Posterior Modelled
Posterior Modelled
Posterior Modelled
March 2013
Observed
April 2013
Observed
May 2013
Observed
Prior Modelled
Prior Modelled
Prior Modelled
Posterior Modelled
Posterior Modelled
Posterior Modelled

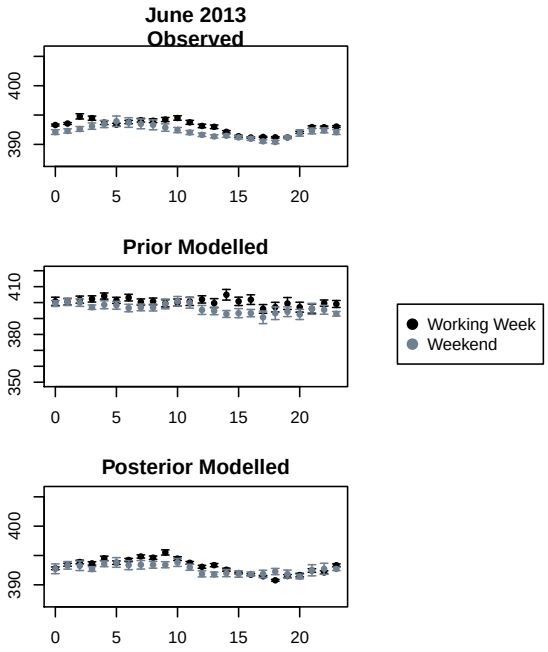

Figure S8. Diurnal cycle of the observed, prior modelled and posterior modelled CO_2 concentrations (ppm) at Hangklip, separated into working week (black) and weekend concentrations (grey), for each month with 95% confidence intervals, where the standard error is calculated over all measurements available for that hour of the day during that particular month.

1.6 Fossil Fuel and NEE Contributions

The contributions of the fossil fuel and NEE fluxes to the modelled concentrations are provided for Robben Island and Hangklip for the months July 2012 to June 2013. As for March 2012 to June 2012, the posterior estimates of the NEE fluxes are increased in such a way that the uptake of CO_2 cancels out the emission of CO_2 due to fossil fuel sources. Little adjustment is made to the contribution from the fossil fuel fluxes to the modelled concentration by the inversion.

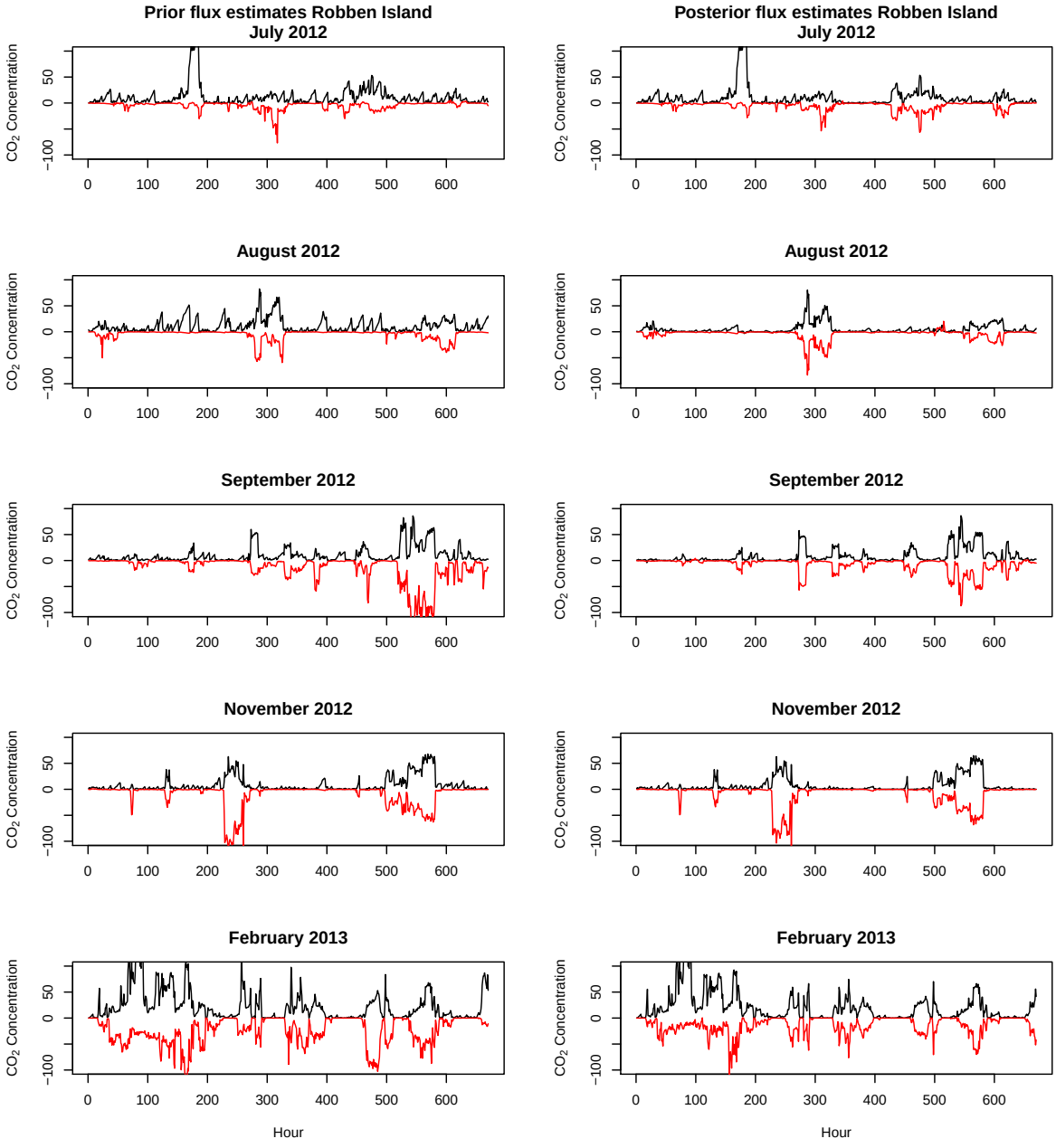
Prior flux estimates Robben Island
July 2012
Posterior flux estimates Robben Island
July 2012
August 2012
August 2012
September 2012
September 2012
November 2012
November 2012
February 2013
February 2013
CO2 Concentration
Hour
−100
0
50
0
100
200
300
400
500
600

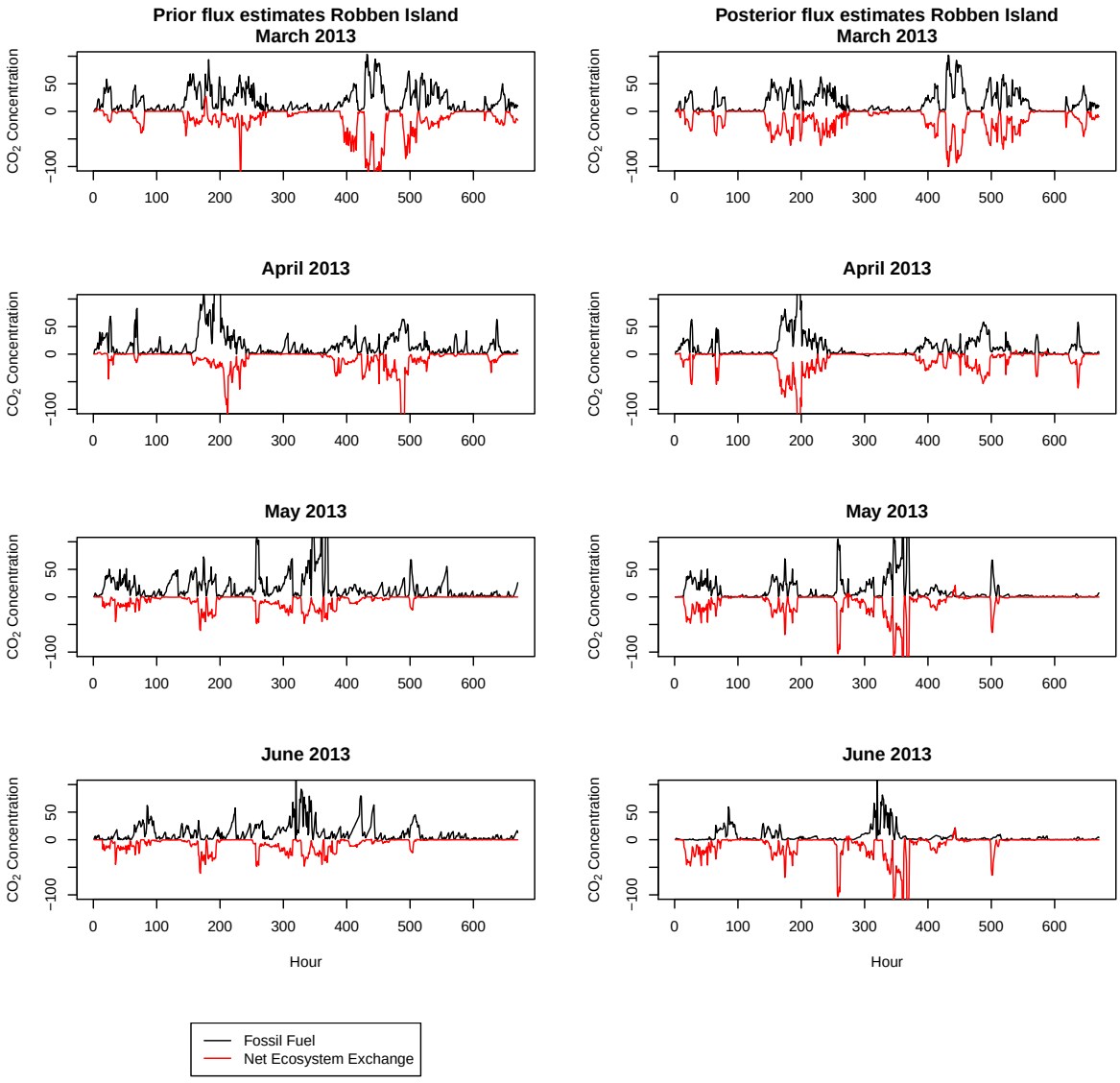

Figure S9. Contribution of the fossil fuel and NEE surface fluxes to the modelled CO_2 concentrations (ppm) at Robben Island.

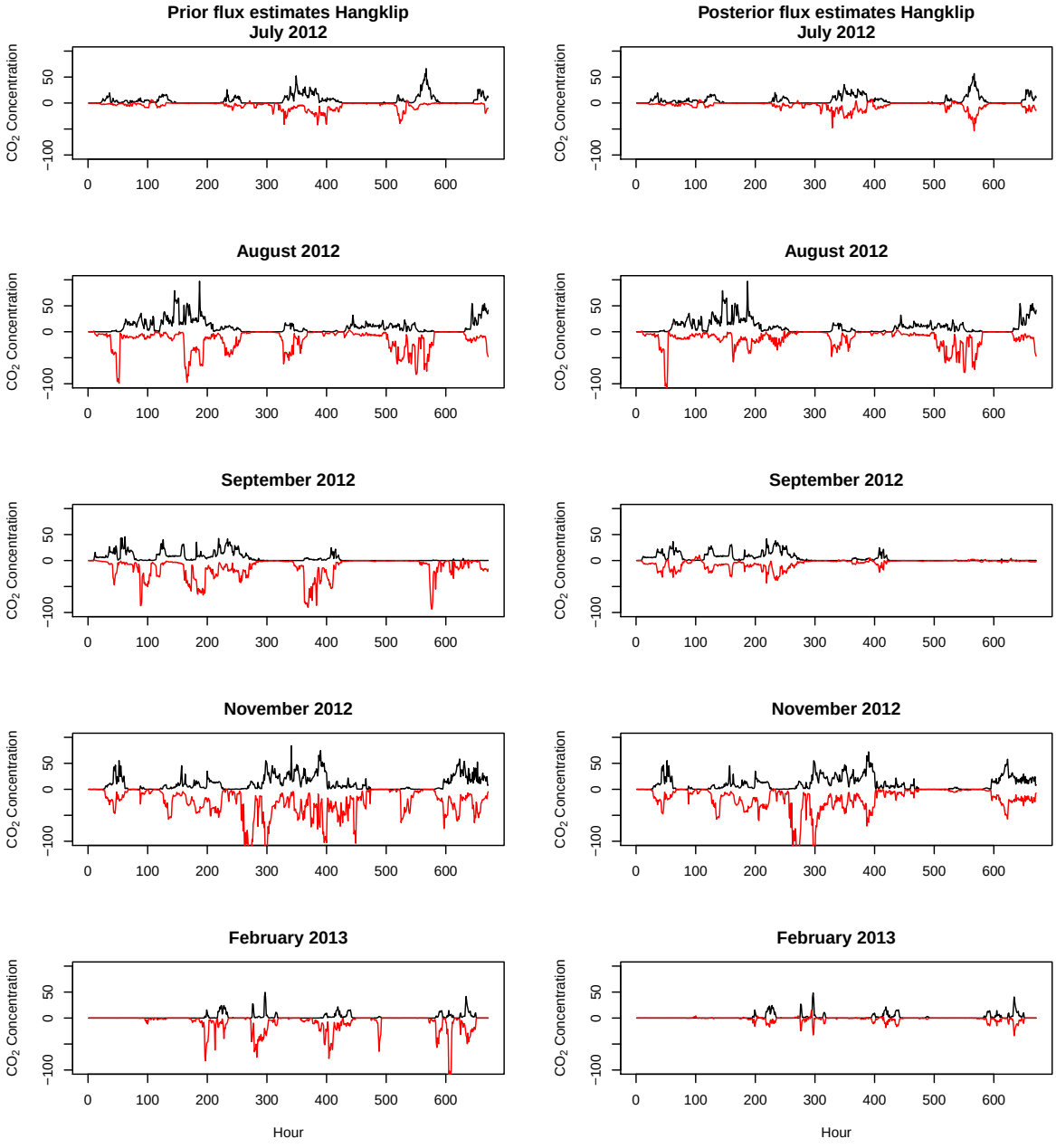
Prior flux estimates Hangklip
July 2012
Posterior flux estimates Hangklip
July 2012
August 2012
August 2012
September 2012
September 2012
November 2012
November 2012
February 2013
February 2013
CO2 Concentration
Hour
−100
0
50
0
100
200
300
400
500
600

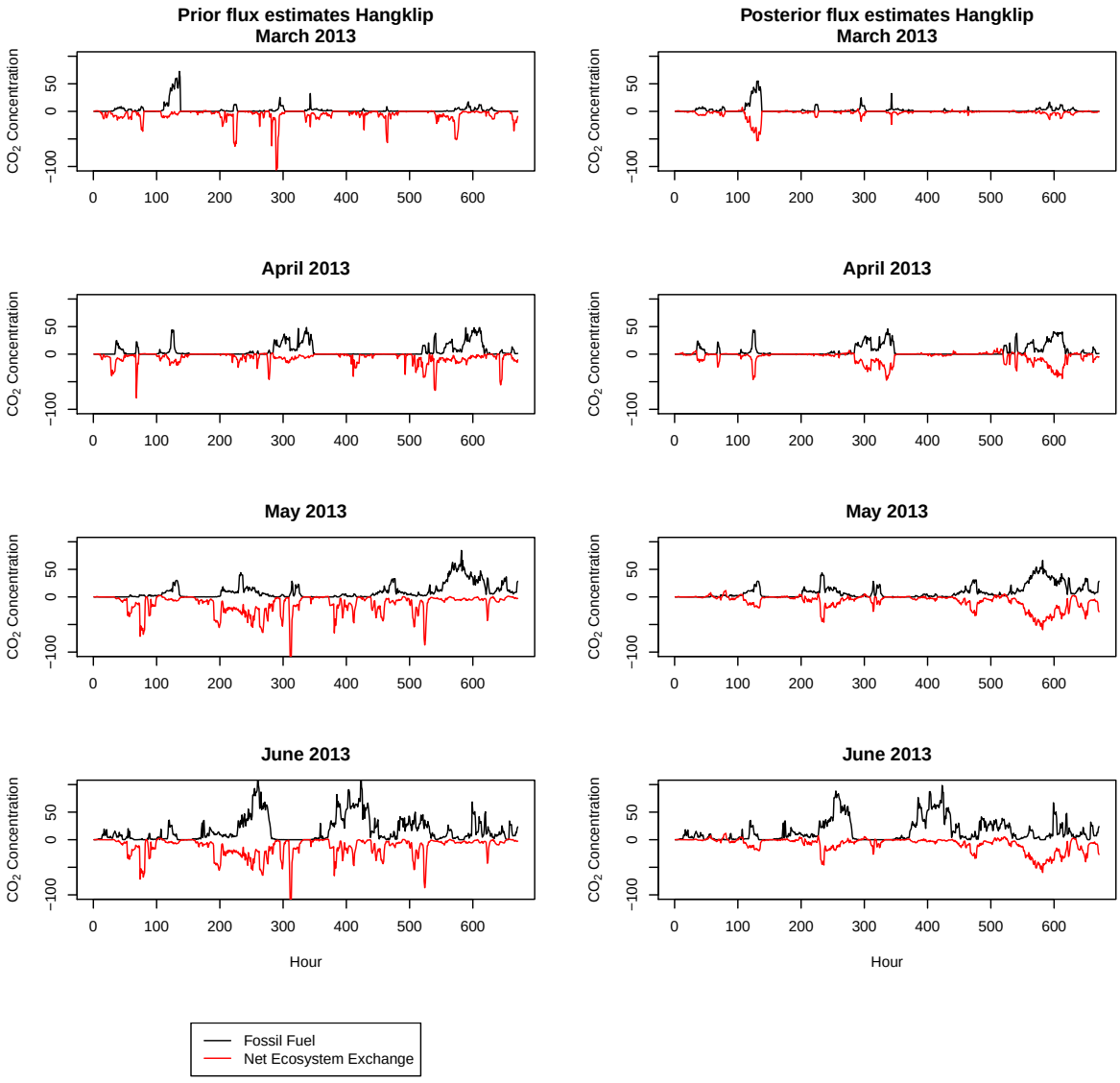

Figure S10. Contribution of the fossil fuel and NEE surface fluxes to the modelled CO_2 concentrations (ppm) at Hangklip.

1.7 Weekly Flux Estimates

Section 3.2 provides a summary of the estimates presented here for the pixel-level weekly fluxes over the full domain for each month.

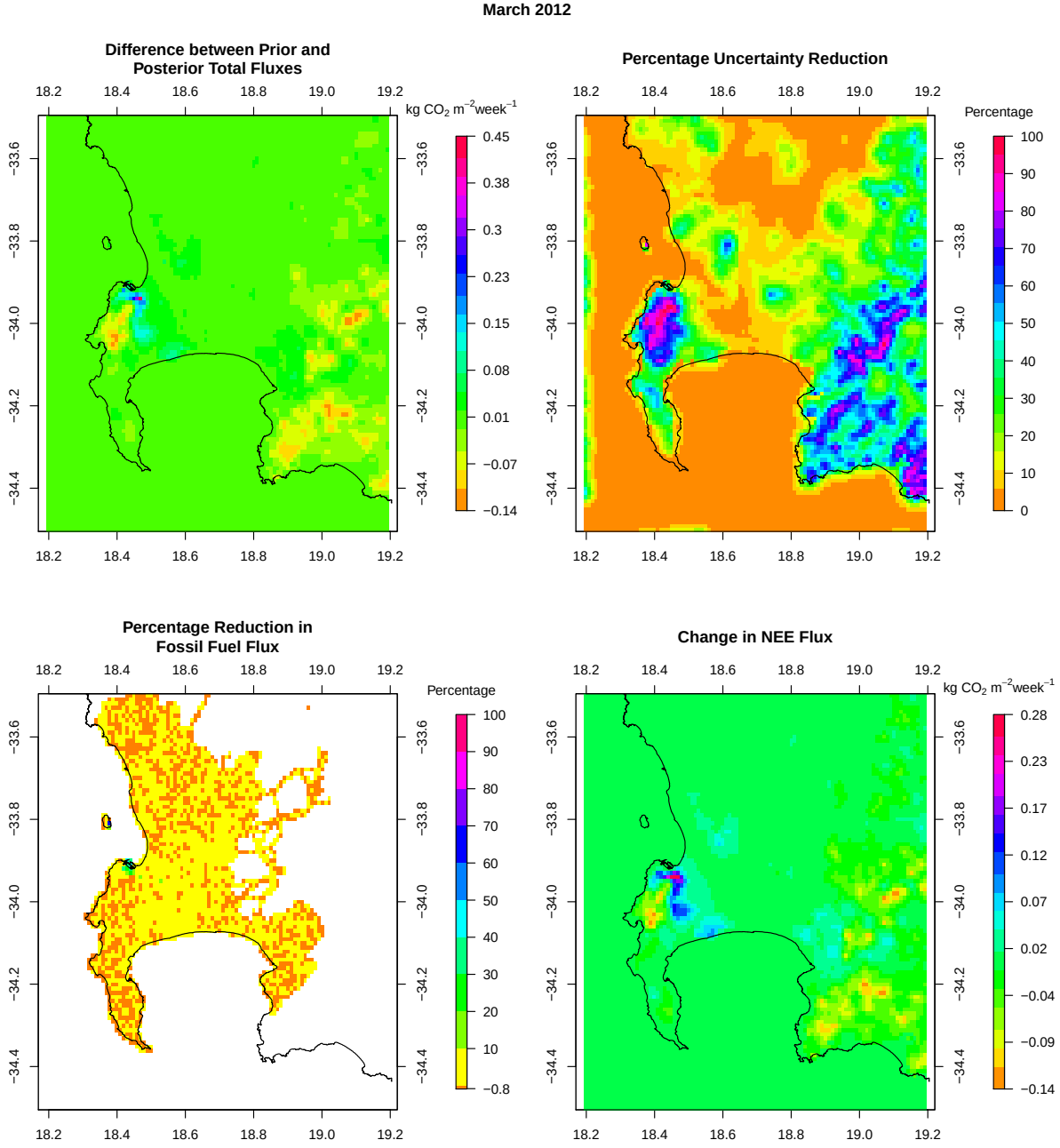

Figure S11. (Top left) Differences between the prior and posterior total flux estimates (kg $CO_2 m^{-2}$ $week^{-1}$) for March 2012 (prior - posterior). (Top right) Percentage reduction in the standard deviation of the flux estimate from prior to posterior. (Bottom left) Percentage reduction in the fossil fuel flux estimates from prior to posterior. (Bottom right) Differences in the biogenic flux estimates between prior and posterior estimates (prior - posterior) (kg $CO_2 m^{-2}$ $week^{-1}$), with negative values indicating posterior CO_2 fluxes were make more positive by the inversion compared with the prior estimates. Extent: between 34.5° and 33.5° S and between 18.2° and 19.2° E.

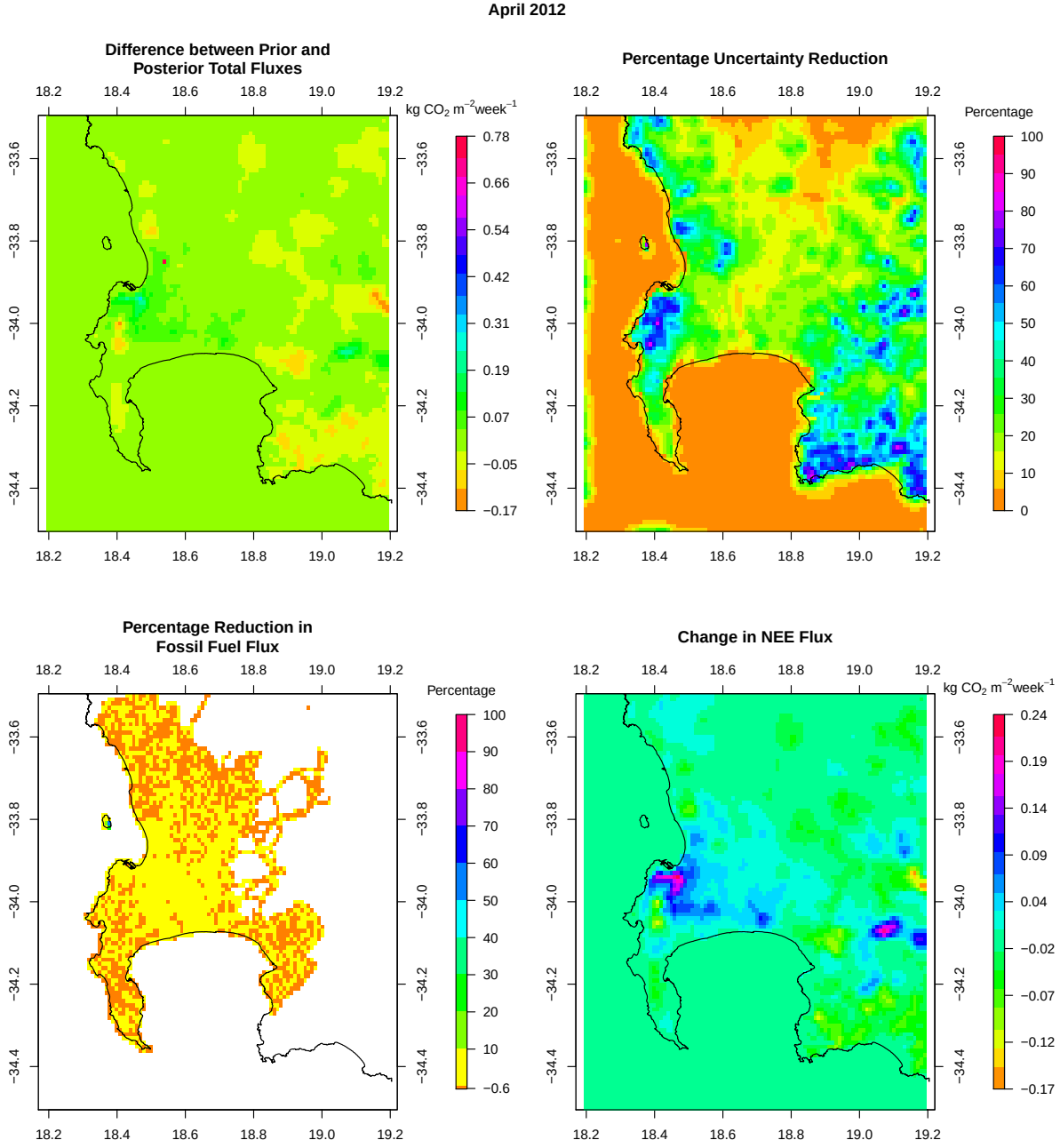

Figure S12. (Top left) Differences between the prior and posterior total flux estimates (kg $CO_2 m^{-2}$ $week^{-1}$) for April 2012 (prior - posterior). (Top right) Percentage reduction in the standard deviation of the flux estimate from prior to posterior. (Bottom left) Percentage reduction in the fossil fuel flux estimates from prior to posterior. (Bottom right) Differences in the biogenic flux estimates between prior and posterior estimates (prior - posterior) (kg $CO_2 m^{-2}$ $week^{-1}$), with negative values indicating posterior CO_2 fluxes were make more positive by the inversion compared with the prior estimates. Extent: between 34.5° and 33.5° S and between 18.2° and 19.2° E.

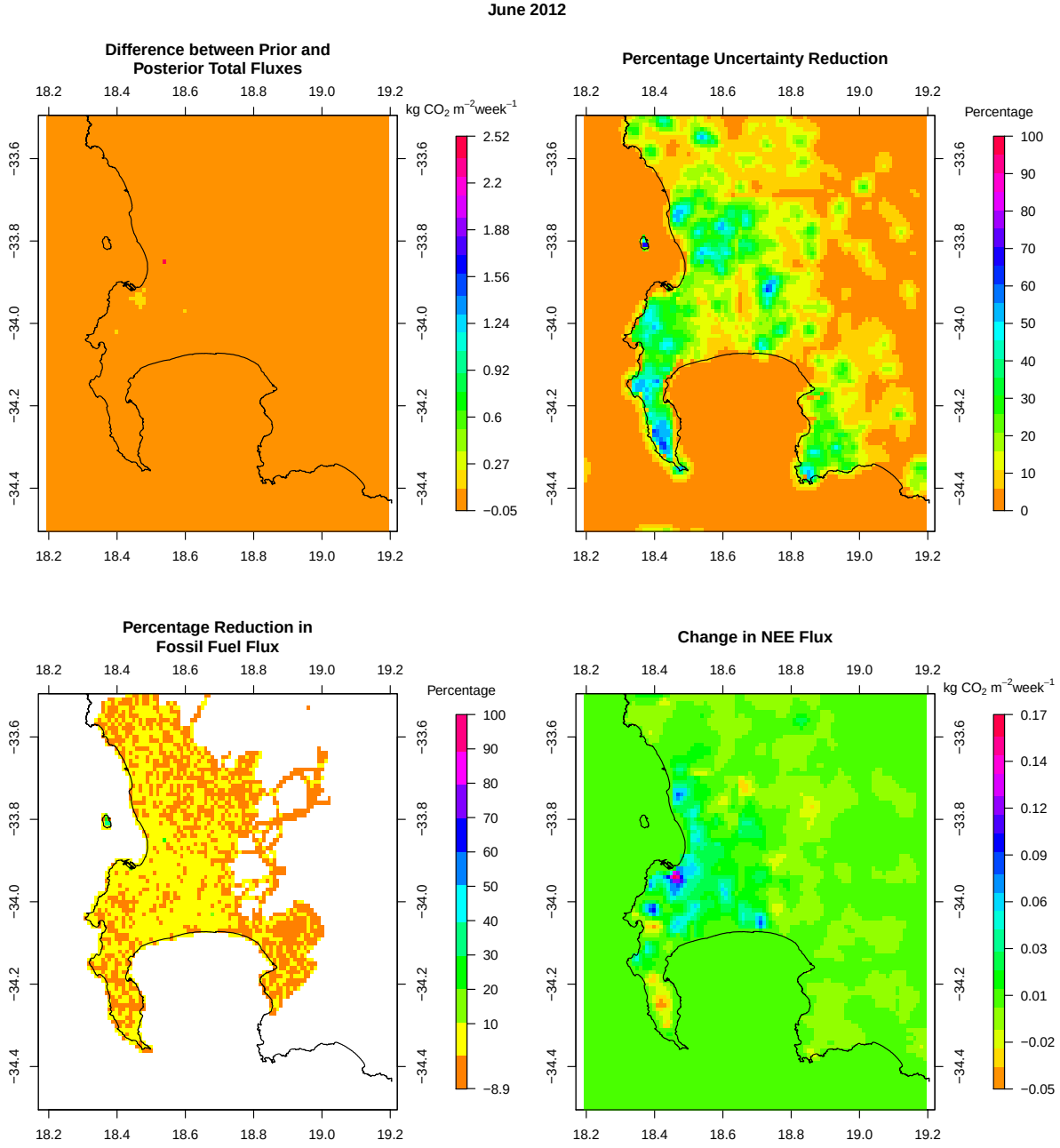

Figure S13. (Top left) Differences between the prior and posterior total flux estimates (kg $CO_2 m^{-2}$ $week^{-1}$) for June 2012 (prior - posterior). (Top right) Percentage reduction in the standard deviation of the flux estimate from prior to posterior. (Bottom left) Percentage reduction in the fossil fuel flux estimates from prior to posterior. (Bottom right) Differences in the biogenic flux estimates between prior and posterior estimates (prior - posterior) (kg $CO_2 m^{-2}$ $week^{-1}$), with negative values indicating posterior CO_2 fluxes were make more positive by the inversion compared with the prior estimates. Extent: between 34.5° and 33.5° S and between 18.2° and 19.2° E.

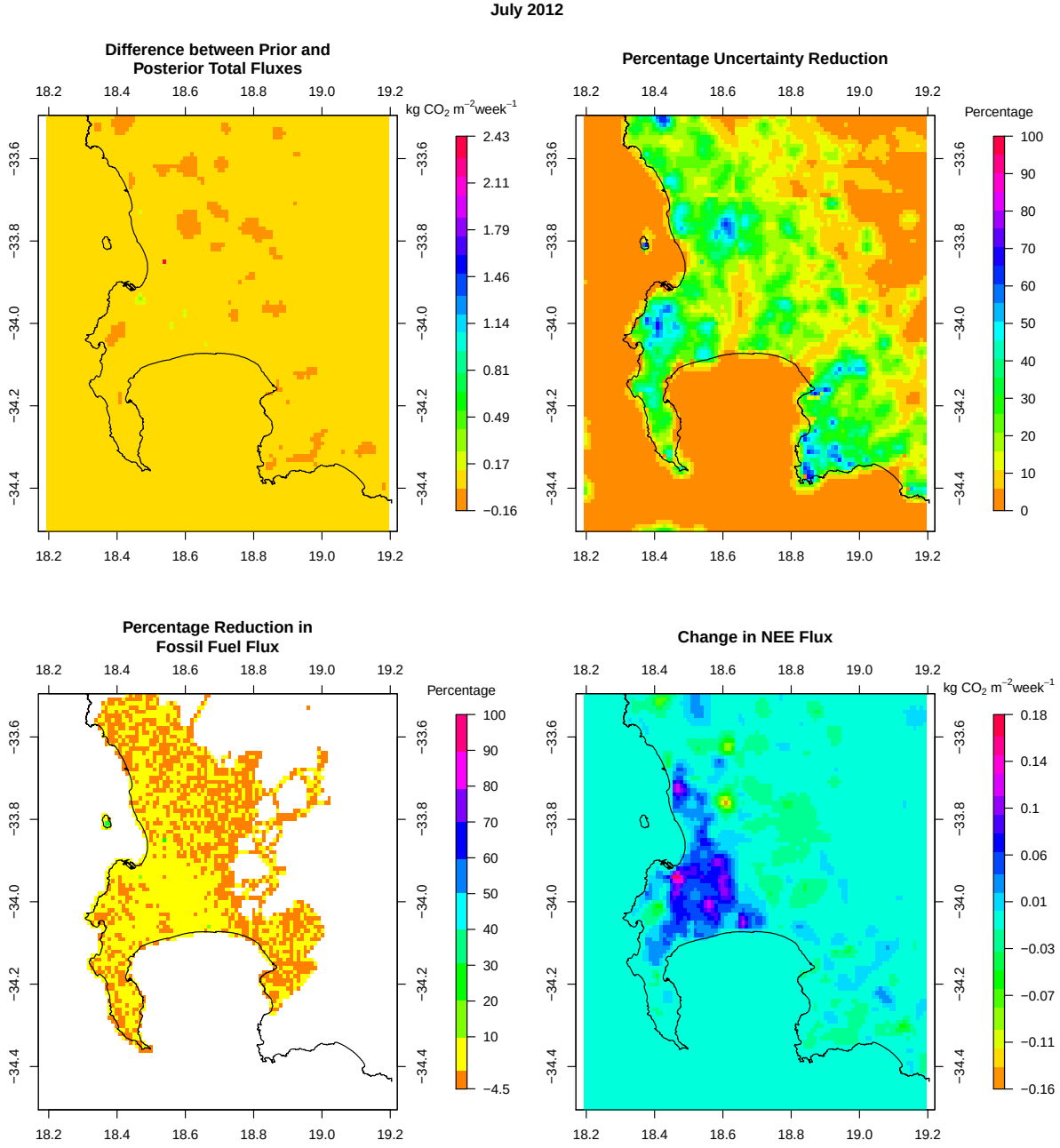

Figure S14. (Top left) Differences between the prior and posterior total flux estimates ($\mathrm{kg\ CO_2 m^{-2}\ week^{-1}}$) for July 2012 (prior - posterior). (Top right) Percentage reduction in the standard deviation of the flux estimate from prior to posterior. (Bottom left) Percentage reduction in the fossil fuel flux estimates from prior to posterior. (Bottom right) Differences in the biogenic flux estimates between prior and posterior estimates (prior - posterior) ($\mathrm{kg\ CO_2 m^{-2}\ week^{-1}}$), with negative values indicating posterior CO_2 fluxes were make more positive by the inversion compared with the prior estimates. Extent: between 34.5° and 33.5° S and between 18.2° and 19.2° E.

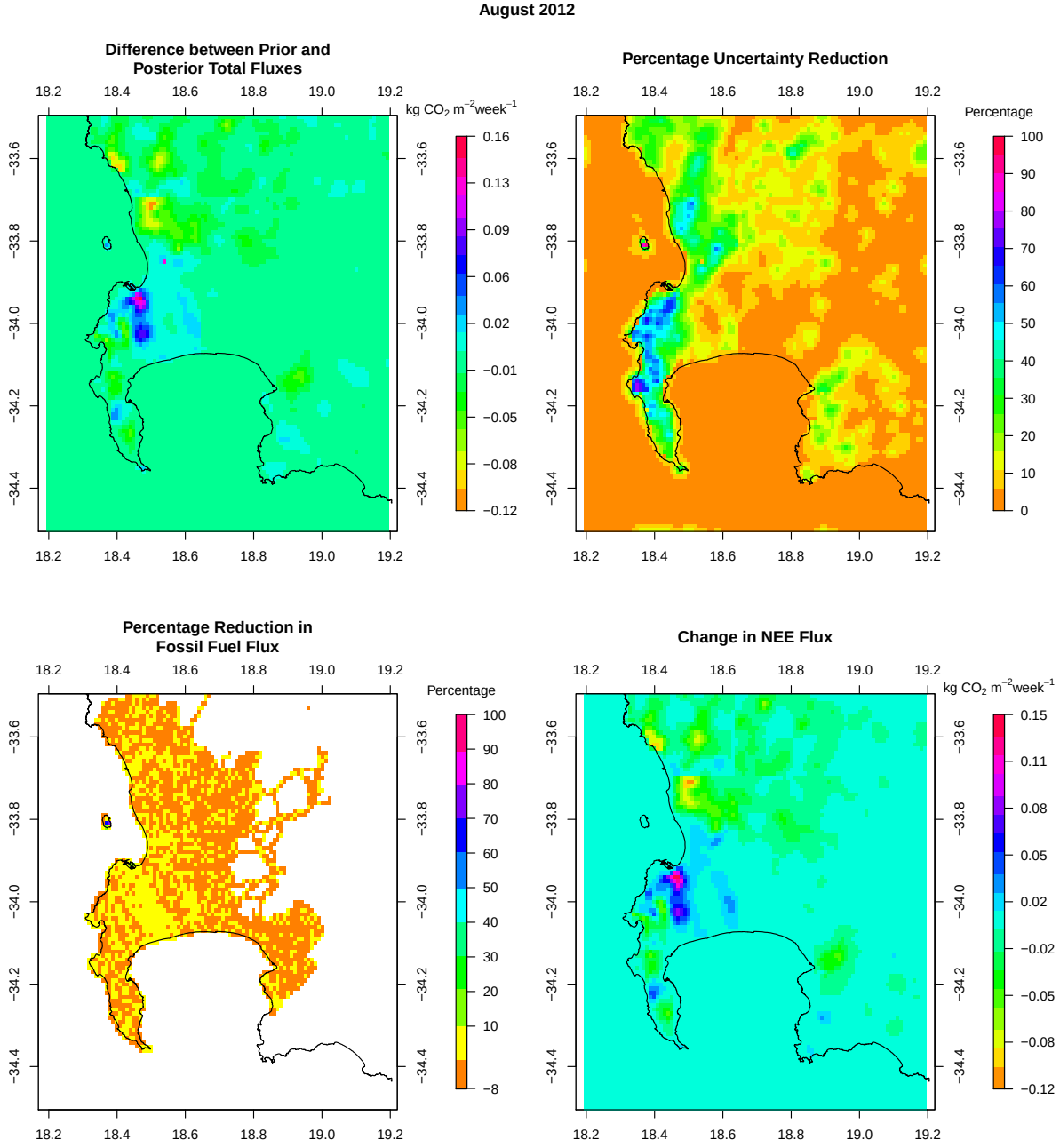

Figure S15. (Top left) Differences between the prior and posterior total flux estimates (kg $CO_2 m^{-2}$ $week^{-1}$) for August 2012 (prior - posterior). (Top right) Percentage reduction in the standard deviation of the flux estimate from prior to posterior. (Bottom left) Percentage reduction in the fossil fuel flux estimates from prior to posterior. (Bottom right) Differences in the biogenic flux estimates between prior and posterior estimates (prior - posterior) (kg $CO_2 m^{-2}$ $week^{-1}$), with negative values indicating posterior CO_2 fluxes were make more positive by the inversion compared with the prior estimates. Extent: between 34.5° and 33.5° S and between 18.2° and 19.2° E.

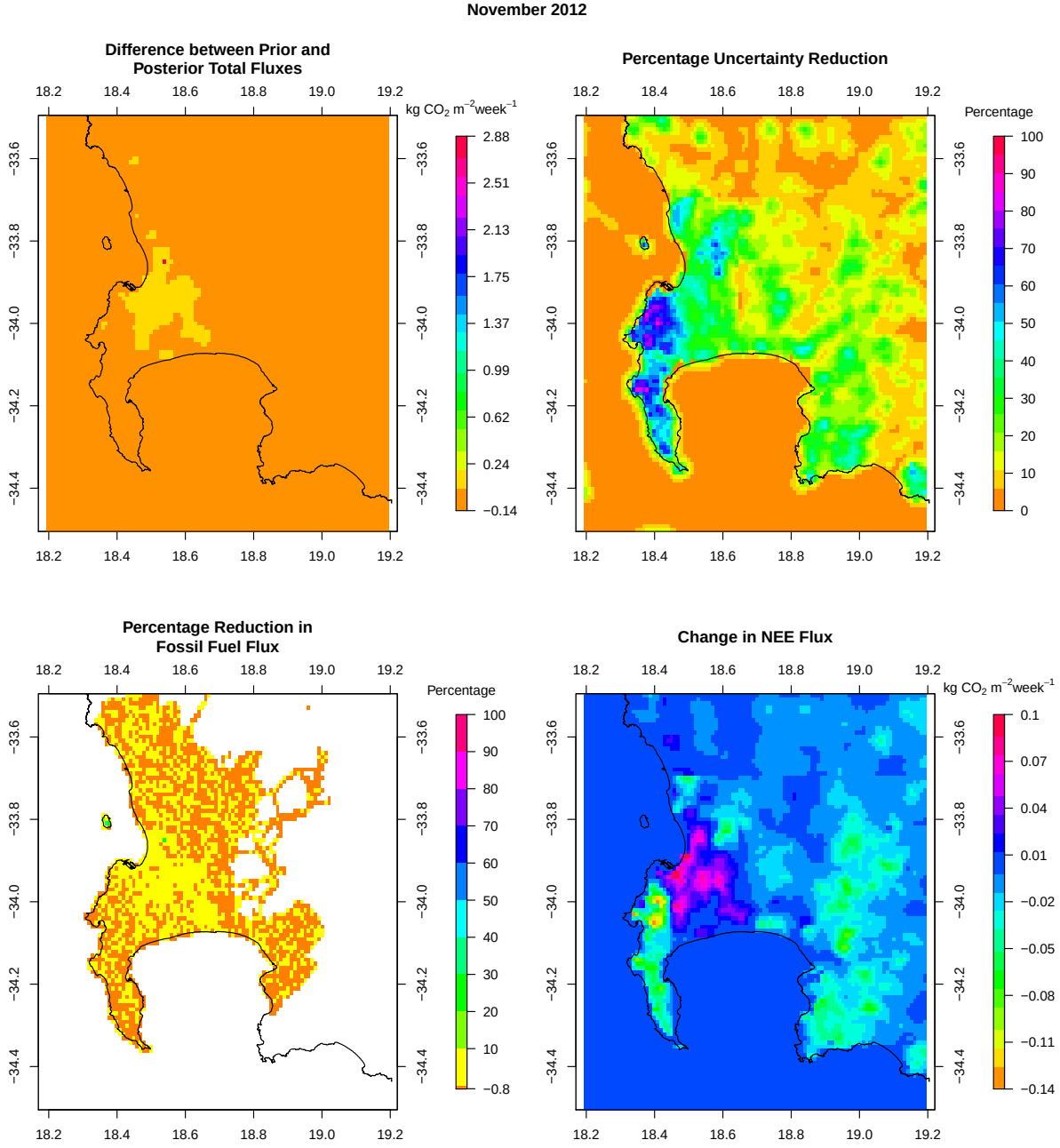

Figure S16. (Top left) Differences between the prior and posterior total flux estimates (kg $CO_2 m^{-2}$ $week^{-1}$) for November 2012 (prior - posterior). (Top right) Percentage reduction in the standard deviation of the flux estimate from prior to posterior. (Bottom left) Percentage reduction in the fossil fuel flux estimates from prior to posterior. (Bottom right) Differences in the biogenic flux estimates between prior and posterior estimates (prior - posterior) (kg $CO_2 m^{-2}$ $week^{-1}$), with negative values indicating posterior CO_2 fluxes were make more positive by the inversion compared with the prior estimates. Extent: between 34.5° and 33.5° S and between 18.2° and 19.2° E.

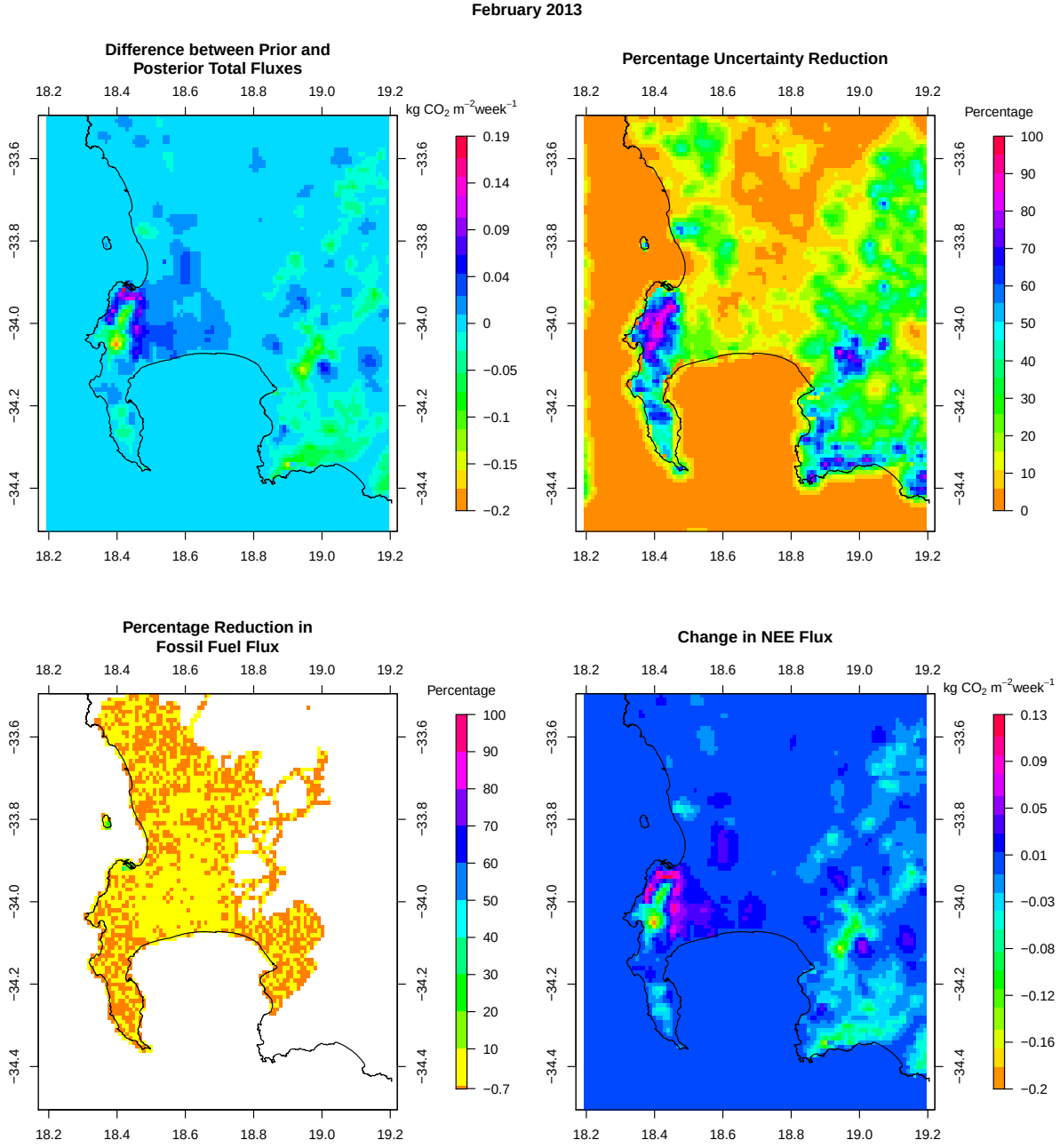

Figure S17. (Top left) Differences between the prior and posterior total flux estimates (kg $CO_2 m^{-2}$ $week^{-1}$) for February 2013 (prior - posterior). (Top right) Percentage reduction in the standard deviation of the flux estimate from prior to posterior. (Bottom left) Percentage reduction in the fossil fuel flux estimates from prior to posterior. (Bottom right) Differences in the biogenic flux estimates between prior and posterior estimates (prior - posterior) (kg $CO_2 m^{-2}$ $week^{-1}$), with negative values indicating posterior CO_2 fluxes were make more positive by the inversion compared with the prior estimates. Extent: between 34.5° and 33.5° S and between 18.2° and 19.2° E.

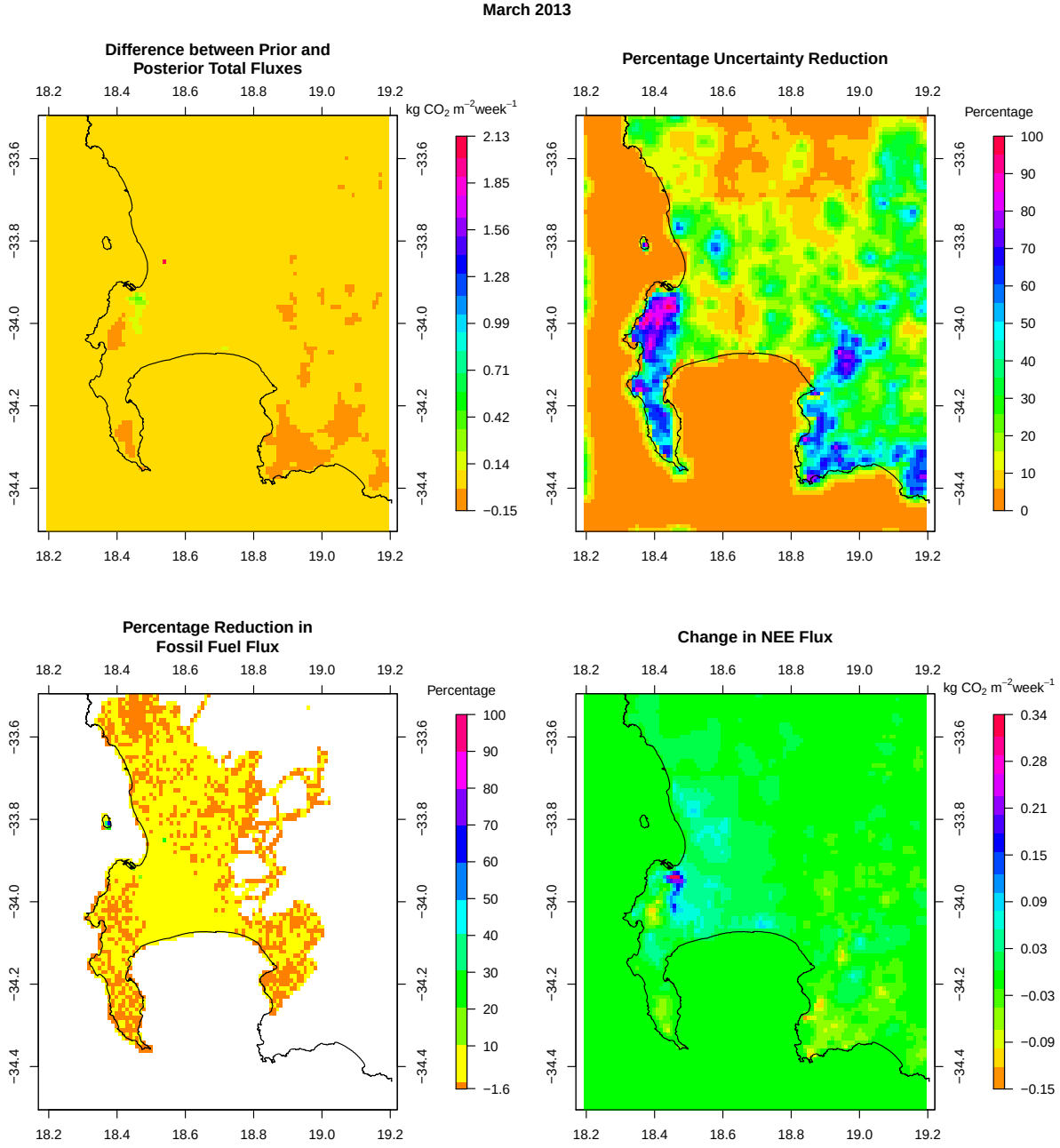

Figure S18. (Top left) Differences between the prior and posterior total flux estimates (kg $CO_2 m^{-2}$ $week^{-1}$) for March 2013 (prior - posterior). (Top right) Percentage reduction in the standard deviation of the flux estimate from prior to posterior. (Bottom left) Percentage reduction in the fossil fuel flux estimates from prior to posterior. (Bottom right) Differences in the biogenic flux estimates between prior and posterior estimates (prior - posterior) (kg $CO_2 m^{-2}$ $week^{-1}$), with negative values indicating posterior CO_2 fluxes were make more positive by the inversion compared with the prior estimates. Extent: between 34.5° and 33.5° S and between 18.2° and 19.2° E.

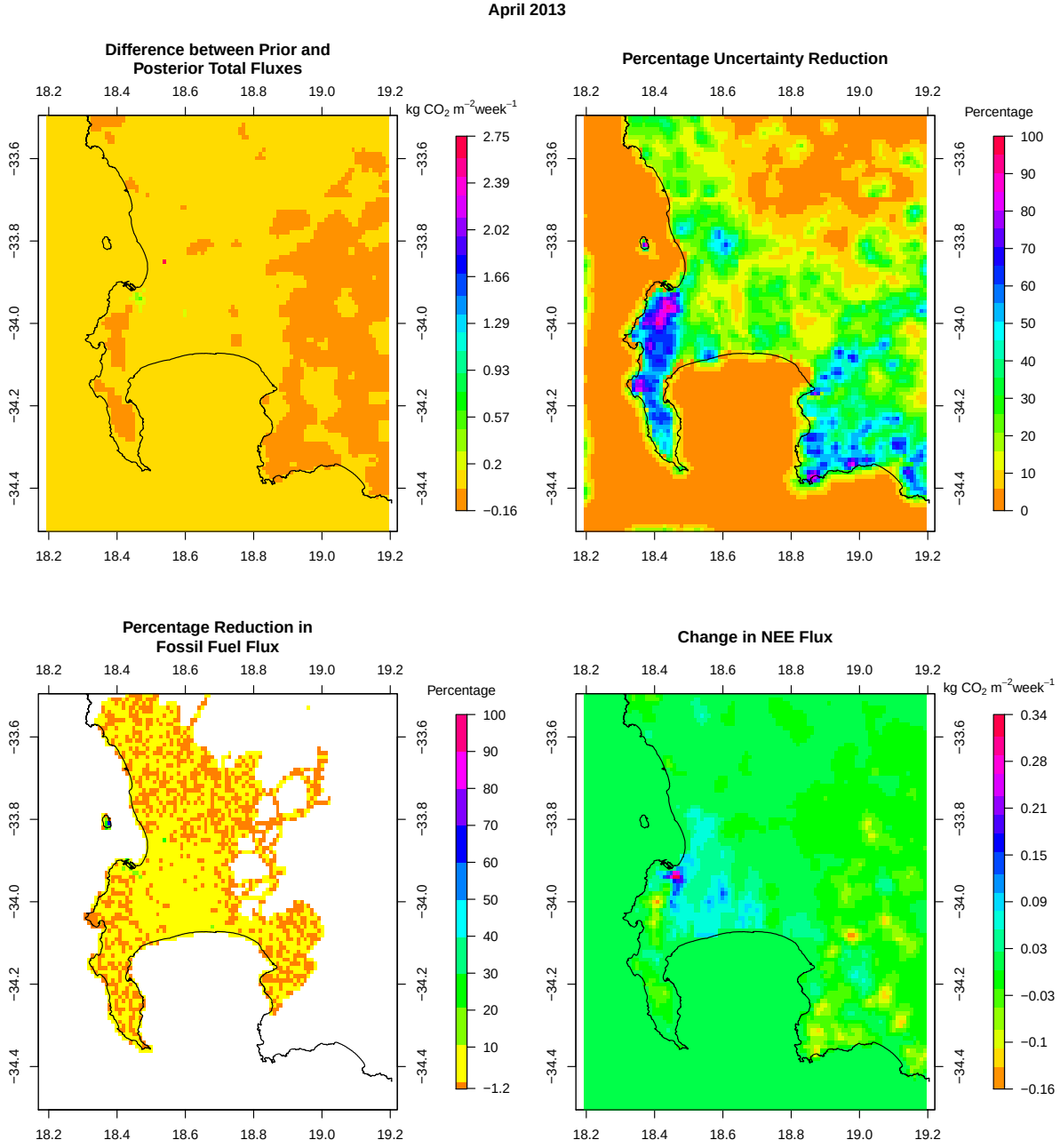

Figure S19. (Top left) Differences between the prior and posterior total flux estimates (kg $CO_2 m^{-2}$ $week^{-1}$) for April 2013 (prior - posterior). (Top right) Percentage reduction in the standard deviation of the flux estimate from prior to posterior. (Bottom left) Percentage reduction in the fossil fuel flux estimates from prior to posterior. (Bottom right) Differences in the biogenic flux estimates between prior and posterior estimates (prior - posterior) (kg $CO_2 m^{-2}$ $week^{-1}$), with negative values indicating posterior CO_2 fluxes were make more positive by the inversion compared with the prior estimates. Extent: between 34.5° and 33.5° S and between 18.2° and 19.2° E.

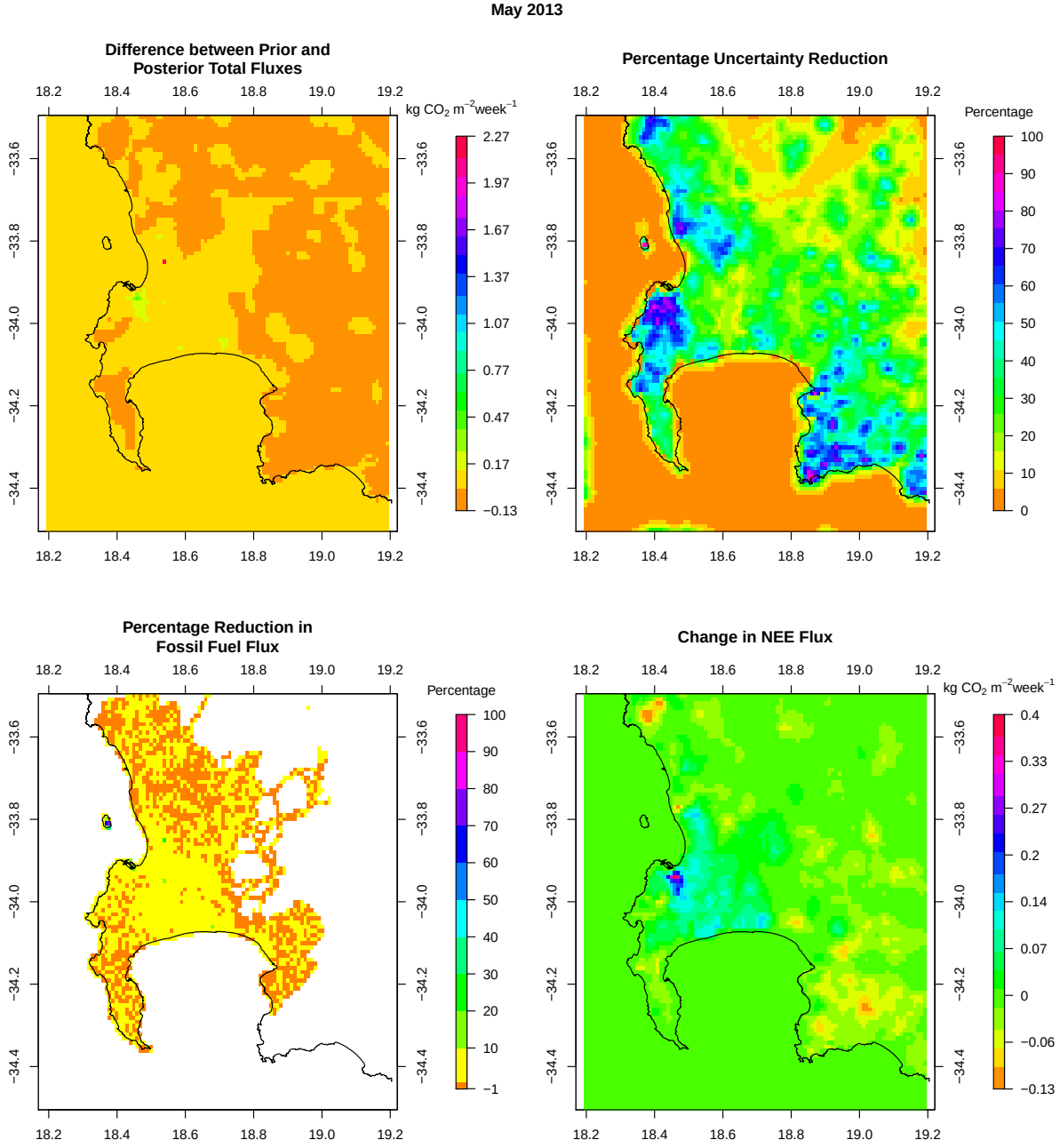

Figure S20. (Top left) Differences between the prior and posterior total flux estimates ($\mathrm{kg\ CO_2 m^{-2}\ week^{-1}}$) for May 2013 (prior - posterior). (Top right) Percentage reduction in the standard deviation of the flux estimate from prior to posterior. (Bottom left) Percentage reduction in the fossil fuel flux estimates from prior to posterior. (Bottom right) Differences in the biogenic flux estimates between prior and posterior estimates (prior - posterior) ($\mathrm{kg\ CO_2 m^{-2}\ week^{-1}}$), with negative values indicating posterior CO_2 fluxes were make more positive by the inversion compared with the prior estimates. Extent: between 34.5° and 33.5° S and between 18.2° and 19.2° E.

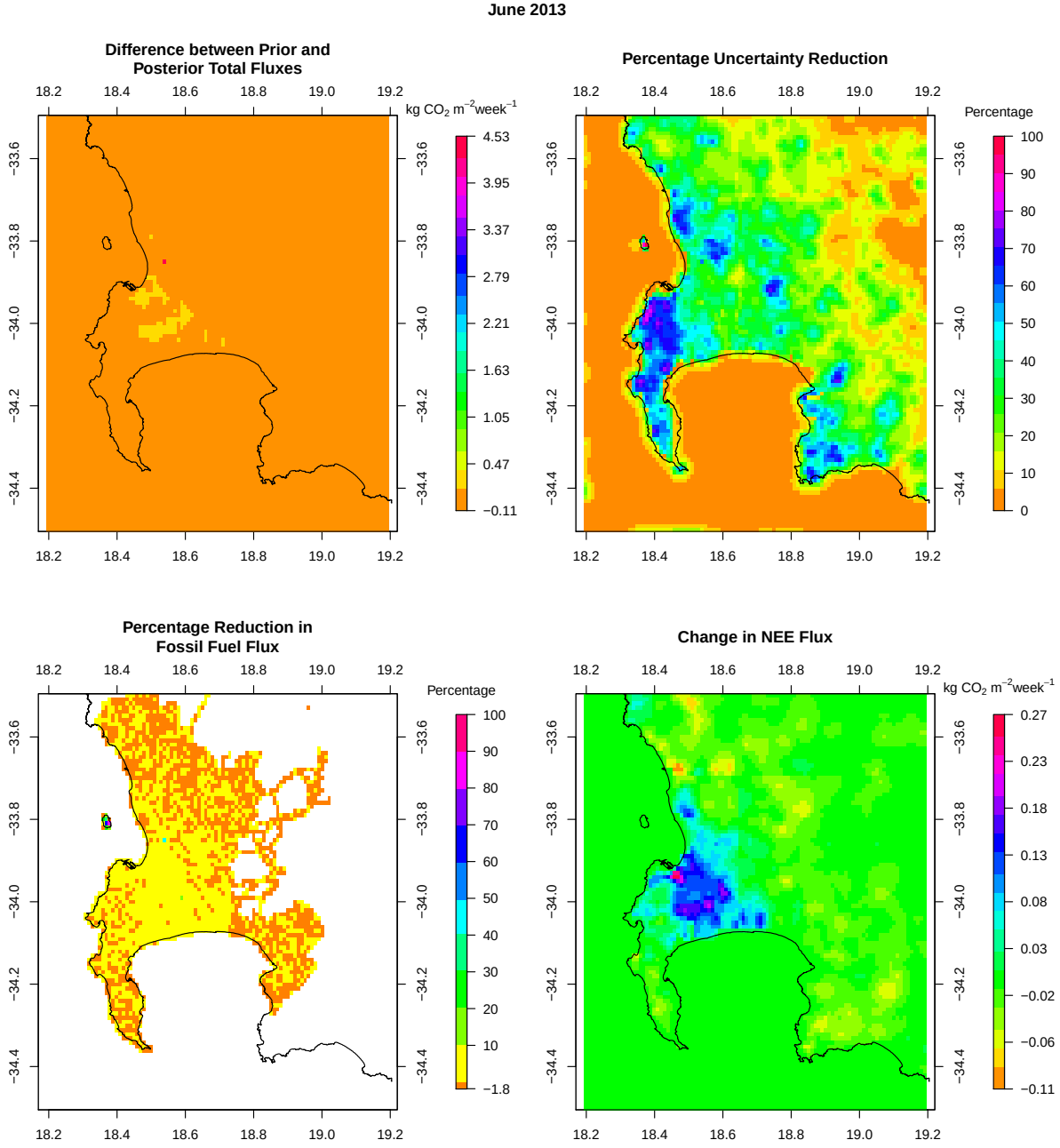

Figure S21. (Top left) Differences between the prior and posterior total flux estimates ($\mathrm{kg\ CO_2 m^{-2}\ week^{-1}}$) for June 2013 (prior - posterior). (Top right) Percentage reduction in the standard deviation of the flux estimate from prior to posterior. (Bottom left) Percentage reduction in the fossil fuel flux estimates from prior to posterior. (Bottom right) Differences in the biogenic flux estimates between prior and posterior estimates (prior - posterior) ($\mathrm{kg\ CO_2 m^{-2}\ week^{-1}}$), with negative values indicating posterior CO_2 fluxes were make more positive by the inversion compared with the prior estimates. Extent: between 34.5° and 33.5° S and between 18.2° and 19.2° E.

1.8 Toy Inversion

Let us consider an hourly measurement at a single site, with a fossil fuel flux daytime source, a fossil fuel flux night-time source, an NEE flux from the same location, and an NEE flux from a neighbouring pixel. We wish to solve for these four fluxes and the covariance matrix of the uncertainties in these fluxes. Selecting some of the most extreme values for the uncertainties and for the sensitivities for the current inversion framework we could get the following:

$$\mathbf{H} = \quad (0.0, 0.0126, 0.00902, 0.0032); \quad \mathbf{C}_{s_0} = \begin{pmatrix} 233 & 0 & 0 & 0 \\ 0 & 78 & 0 & 0 \\ 0 & 0 & 1578 & 1220 \\ 0 & 0 & 1220 & 1578 \end{pmatrix}; \quad \mathbf{C}_c = 4$$

Solving for the posterior covariance matrix of the flux uncertainties using:

$$\mathbf{C}_s = \left(\mathbf{H}^T {\mathbf{C}_c}^{-1} \mathbf{H} + {\mathbf{C}_{s_0}}^{-1}\right)^{-1} \tag{1}$$

$$= \mathbf{C}_{s_0} - \mathbf{C}_{s_0} \mathbf{H}^T \left(\mathbf{H} \mathbf{C}_{s_0} \mathbf{H}^T + \mathbf{C}_c\right)^{-1} \mathbf{H} \mathbf{C}_{s_0}. \tag{2}$$

gives

$$\mathbf{C}_s = \begin{pmatrix} 233 & 0 & 0 & 0 \\ 0 & 77.8 & -4.2 & -3.7 \\ 0 & -4.2 & 1500.2 & 1151.1 \\ 0 & -3.7 & 1151.1 & 1517.0 \end{pmatrix}; \quad \rho_{\mathbf{matrix}} = \begin{pmatrix} 1 & 0 & 0 & 0 \\ 0 & 1 & -0.01 & -0.01 \\ 0 & -0.01 & 1 & 0.76 \\ 0 & -0.01 & 0.76 & 1 \end{pmatrix};$$

Although the sensitivity of the concentration measurement to the fossil fuel and NEE fluxes are not that different, the posterior covariances are small because the transport Jacobian only projects fluxes from individual pixels weakly into modelled concentrations. The uncertainties in the prior modelled concentrations that are attributed to the flux contributions ($\mathbf{H}\mathbf{C}_{s_0}\mathbf{H}^T$) are small relative to the uncertainties specified for the modelled concentration errors ($\mathbf{C}_c$). If we reduce the elements of $\mathbf{C}_c$ then the posterior covariances increase. For example, If $\mathbf{C}_c$ = 1 then

$$\mathbf{C}_s = \begin{pmatrix} 233 & 0 & 0 & 0 \\ 0 & 77.2 & -14.5 & -12.9 \\ 0 & -14.5 & 1310.0 & 982.8 \\ 0 & -12.9 & 982.8 & 1368.0 \end{pmatrix}; \quad \rho_{\mathbf{matrix}} = \begin{pmatrix} 1 & 0 & 0 & 0 \\ 0 & 1 & -0.04 & -0.04 \\ 0 & -0.04 & 1 & 0.73 \\ 0 & -0.04 & 0.73 & 1 \end{pmatrix};$$

References

Lamigueiro, O., P.: Visualization methods for raster data, ver. 0.41. http://oscarperpinan.github.io/rastervis